




# Review of isomers in the $A \approx 135$ region and nuclear shape evolution

R. Palit<sup>1,a</sup> , Md. S. R. Laskar<sup>1,2</sup>, S. Nag<sup>3</sup>, D. Choudhury<sup>4</sup>, N. Goel<sup>3</sup>, S. Singh<sup>4</sup>, and S. N. Mishra<sup>5</sup>

<sup>1</sup> Department of Nuclear and Atomic Physics, Tata Institute of Fundamental Research, Mumbai 400005, India

<sup>2</sup> Istituto Nazionale di Fisica Nucleare (INFN), Sezione di Milano, Milan 20133, Italy

<sup>3</sup> Department of Physics, Indian Institute of Technology (BHU), Varanasi 221005, India

<sup>4</sup> Department of Physics, Indian Institute of Technology, Ropar, Punjab 140001, India

<sup>5</sup> Indian Institute of Science Education and Research, Berhampur 760010, India

Received 20 March 2024 / Accepted 2 May 2024 / Published online 23 May 2024

© The Author(s) 2024

**Abstract** The measurements of lifetimes and electromagnetic moments of the isomeric states in some of the nuclei around  $A \approx 135$  carried out at BARC-TIFR Pelletron Linac Facility at TIFR, Mumbai, are highlighted. The results from these measurements, along with similar studies reported in the literature, provide a wealth of nuclear structure information in Ba, La, and Ce isotopes in the  $A \approx 135$  region. Comparison of the measured moments with the calculations gives a unique testing ground for the predictive power of the nuclear models. Plans for similar studies in other mass regions are also described at the end.

## 1 Introduction

An isomer, a metastable state of a nucleus with a lifetime greater than 1 ns, is caused due to the hindrance of the decay process back to lower excited states. There are mainly three reasons posing the hindrance on the isomeric decays, the first reason being the different structural wave functions of the initial and final states. The other two reasons posing the hindrance are the small decay energy and the large change in angular momentum. The isomers can be classified into spin and seniority isomers in spherical regions, on the basis of the type of hindrance mechanisms on their respective decays. In deformed regions, the isomers are categorized as shape,  $K$  and fission isomers, where  $K$  denotes the total angular momentum projection on the symmetry axis for axially deformed nuclei [1–4]. Nuclear isomers are produced within the same nucleus ( $N$ ,  $Z$ ) due to the different arrangement of nucleons. Isomers are crucial in basic nuclear structure studies, nuclear astrophysics as well as energy storage in isomeric states. These isomeric states play an important role in testing the predictions of shell and collective models for nuclear structure. The isomeric lifetime is also necessary in experiments such as Time Differential Perturbed Angular Distribution (TDPAD), to extract the  $g$ -factor or electric quadrupole moment of the excited state [5]. Nuclear moments are very sensitive probes to understand the detailed composition of the nuclear wave function.

Of particular interest are the isomers in transitional nuclei in  $A \approx 135$  region which can be probed by low energy stable beam accelerator. The nuclear structure evolves from spherical to deformed shapes as one goes away from the shell gap. The high spin structure of transitional nuclei, which lie between the spherical and deformed ones, is of particular importance as they pose a challenge to various nuclear models. Experimental studies of nuclei in the vicinity of closed shells are ideal for testing the predictions of continuously evolving shell model calculations based on effective interactions, as well as the projected shell model calculations. With the recent development of large-scale shell model calculations near  $A \approx 130$  regions [6], it is now possible to study some of these transitional and closed-shell nuclei using the same effective interactions. Studies of these nuclei near  $N = 82$  shell gap are currently an active subject of nuclear structure research and have attracted extensive experimental as well as theoretical attention in recent years [7–14]. The  $Z > 50$  transitional nuclei around  $A \approx 135$ , for  $N < 82$ , lie between the spherical and deformed regions. These nuclei show rich and complex level structures because of the interplay between single-particle and collective modes of excitation. The occupation of high- $j$  orbitals for protons and neutrons is responsible for various structural phenomena for nuclei in this region, such as magnetic and chiral

<sup>a</sup> e-mail: [palit@tifr.res.in](mailto:palit@tifr.res.in) (corresponding author)

rotations, wobbling motion, and high-spin isomers. Many high-spin isomers have been reported in nuclei around  $A \approx 135$  with neutron numbers close to  $N = 82$  shell closure having simple multi-quasiparticle configurations [10, 15–17].

The lanthanum isotopes are enriched with lots of low- and high-spin isomers. In particular, these isomers will provide insight into the evolution of the nuclear structure of lanthanum isotopes approaching the  $N = 82$  shell gap from the mid-shell region. A series of experiments have been carried out at the Pelletron Linac Facility (PLF) at Tata Institute of Fundamental Research (TIFR), Mumbai, to study the isomers in La isotopes. Similar studies on  $^{135, 136}\text{La}$  have been reported by the Research Center for Nuclear Physics (RCNP), Osaka University, [15, 16] using the radioactive beam of  $^{17}\text{N}$ . In addition, we want to see if some of the isomers in La isotopes would relate to the isomers in neighboring even–even isotopes of Ba and Ce. These would provide insight into the structural evolution in this region as one approaches the  $N = 82$  shell gap from the mid-shell region in view of isomers.

We have organized the manuscript in the following way. The experimental results on La isotopes are presented in Sect. 2 along with the description of the setups at PLF. Section 3 provides a systematic study of isomers in Ce and Ba and their role in shape evolution. In Sect. 4, we discuss the coupling of an odd neutron or odd proton to the isomers in an even–even core to explain the structure of some of the isomers in odd-Ba or odd-Ce as well as odd-La isotopes. Section 5 provides future plans for similar studies in other mass regions. In Sect. 6, we present the conclusions.

## 2 Isomers in La nuclei

The  $Z = 57$  lanthanum isotopes are enriched with lots of low- and high-spin isomers. These isomers provide useful insight into the evolution of the nuclear structure of the lanthanum isotopes as we move toward the  $N = 82$  shell closure. Recently, a longitudinal wobbling band has been found in  $^{133}\text{La}$ , feeding the  $11/2^-$  isomeric state in  $^{133}\text{La}$  [9, 18]. The measurement of the nuclear moment of the  $11/2^-$  isomeric state is needed to understand the structure of  $^{133}\text{La}$ .

A series of experiments were performed at the BARC-TIFR 14UD pelletron linac accelerator facility (PLF) at Mumbai, using heavy-ion fusion-evaporation reaction for the lifetime and moment measurements in La isotopes. There are two experimental setups. One is for  $\gamma$ -ray spectroscopy using a hybrid array of Compton-suppressed clover HPGe detectors coupled with  $\text{LaBr}_3(\text{Ce})$  scintillator detectors. The other is for the time differential perturbed angular distribution (TDPAD) measurement. Brief descriptions of the setups are given below along with the experimental results.

### 2.1 Hybrid array at PLF and results on lifetime measurements in La isotopes

The detector array at TIFR has the provision to accommodate 24 Compton-suppressed HPGe clover detectors and 18  $\text{LaBr}_3(\text{Ce})/\text{CeBr}_3(\text{Ce})$  detectors for fast timing measurements. A schematic diagram of the experimental setup is shown in Fig. 1.

A root-based multi-threaded software named “TIFR Digital Data Acquisition Software for Nuclear Structure Studies (TIDES)” developed at TIFR [19], was used to acquire data and control the data acquisition system coupled to this hybrid array. This hybrid Indian National Gamma Array (INGA) [20, 21] spectrometer has the capability to perform lifetime measurements of excited nuclear states in the 50 ps – 2  $\mu\text{s}$  range to extract information on nuclear structure and isomers.

Several studies have been carried out for the lanthanum isotopes populating the La nuclei using  $^{11}\text{B}$ -induced reactions on different enriched Te isotopes. For the study of the excited states of  $^{137}\text{La}$ , the fusion evaporation reaction  $^{130}\text{Te}(^{11}\text{B}, 4n)$  at a beam energy of 40 MeV was used. The work has been reported by Laskar et al., in 2021 [22], where all the experimental details are described. Prior to this work, only an upper limit of the half-life for the  $11/2^-$  state in  $^{137}\text{La}$  was reported as  $T_{1/2} \leq 410(70)$  ps [23]. The  $\gamma$ -rays decaying from the  $11/2^-$  state reported in this work were found to be consistent with Ref. [24], which reported a weak transition of 87.2 keV in addition to 169.4-, 993.7- and 1004.6-keV transitions mentioned in the other earlier works on  $^{137}\text{La}$  [23, 25, 26]. Laskar et al. [22] reported a re-measurement of the lifetime for this state using the hybrid array. To get the time spectrum, the energy gate from the HPGe clover detectors was used to select the cascade of  $\gamma$  rays across this 1004.6-keV state in  $\text{LaBr}_3(\text{Ce})$ .

The half-life, on fitting the time spectrum with the function of

$$I(t) = A \exp\left(\frac{\sigma^2}{2\tau^2} - \frac{t}{\tau}\right) \left[1 - \text{erf}\left(\frac{\sigma^2 - \tau t}{\sqrt{2}\sigma\tau}\right)\right] \quad (1)$$

was reported as  $263 \pm 12$  ps for the  $11/2^-$  [22], as shown in Fig. 2. It is interesting to note that this half-life is

**Fig. 1** The geometry of the part of the hybrid INGA consisting of 24 Compton suppressed clover HPGe and 18 LaBr<sub>3</sub>(Ce) detectors in GEANT4

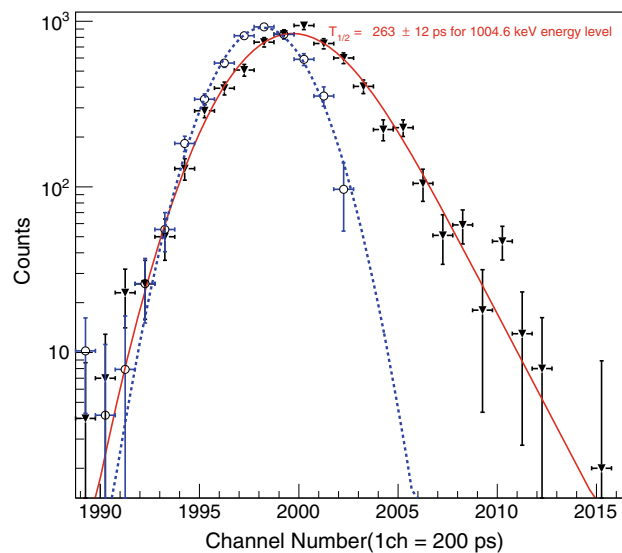
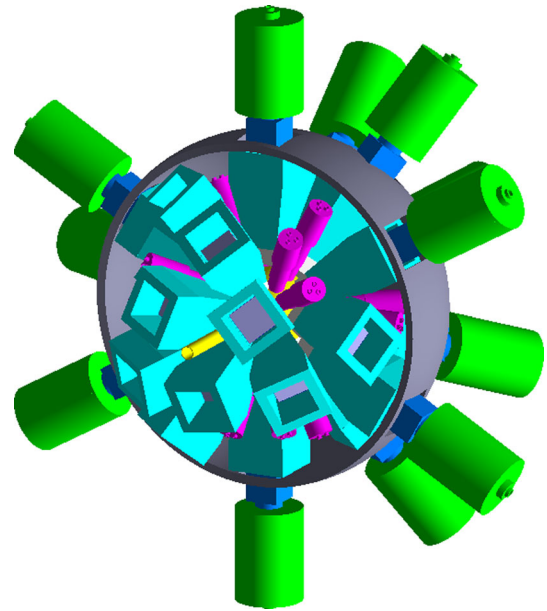


**Fig. 2** Time difference spectrum (filled triangle) between LaBr<sub>3</sub>(Ce) detectors with  $\gamma$  gated on HPGe, while 169.4 keV at the start  $-782$  keV at the stop in LaBr<sub>3</sub>(Ce) along with the fitted function (red colour solid line) with exponential convoluted by Gaussian function, giving  $T_{1/2} = 263 \pm 12$  ps for 1004.6 keV energy level. Time difference spectrum (open circle) with a start at 94 keV and stop at 455 keV from  $^{137}\text{La}$  nucleus along with fitted Gaussian function (blue dotted line) showed FWHM=  $985 \pm 23$  ps (taken from Ref. [22])

smaller than those in  $^{129,131,133}\text{La}$  isotopes. The lifetimes of the  $11/2^-$  states in  $^{135,139}\text{La}$  are not yet known which calls for new measurements in these nuclei.

## 2.2 TDPAD setup at PLF and g-factor measurements

The  $g$ -factors of the isomeric states have been measured using the time differential perturbed angular distribution (TDPAD) method at the PLF facility. The magnetic moment measurements were carried out using a split-coil superconducting magnet provided by American Magnetics, Inc. (AMI), which is capable of producing magnetic fields up to 7 T. The magnet is designed to have field stability of better than 0.1% and uniformity of 0.5% over a 1 cm diameter spherical volume (dsv).

A pulsed beam was used for these measurements. Each beam pulse had a width of  $\sim 1$  ns, and 800 ns separation between the consecutive beam bunches. The delayed  $\gamma$  rays from the isomers were measured by four single crystal HPGe detectors placed around the target at angles  $\pm 45^\circ$  and  $\pm 135^\circ$  with respect to the beam direction. The distance between the detectors and the target center was 11 cm. The time resolution (full width at half maximum (FWHM) of the prompt-peak) in the time spectrum of the detectors was found to be about 5 ns for the 1173- and 1332- keV transitions of  $^{60}\text{Co}$  radioactive source. The time-to-amplitude converter (TAC) was started using the time signal from the HPGe detector. The TAC was stopped by the primary RF signal of the buncher. The data were collected in LIST mode with eight parameters for energy and time signals from the four detectors. In the offline analysis, two-dimensional spectra with energy vs. time were constructed for each detector. The time difference spectra for the  $\gamma$ -rays decaying from the isomeric state were generated by taking energy-gated time projections. Normalized counts for each detector  $N(\theta, t)$  were used to construct the spin rotation spectra defined as

$$R(t) = [N \uparrow(\theta, t) - N \downarrow(\theta, t)] / [N \uparrow(\theta, t) + N \downarrow(\theta, t)] \quad (2)$$

The form of  $R(t)$  depends on the geometry of the experimental setup and hyperfine interactions present due to a magnetic dipole, or an electric quadrupole, or both [27, 28]. For a pure magnetic dipole interaction, the spin rotation function for the experimental geometry used in the measurements with the PLF is expressed as [29]

$$R(t) = A_2 G_2(t) = -\frac{3}{4} A_2 \sin(2\omega_L t - \phi) \exp(-\lambda t) \quad (3)$$

where,  $A_2$  is the amplitude,  $G_2(t)$  is the perturbation function due to magnetic hyperfine interaction with Larmor frequency  $\omega_L$ , and  $\lambda$  is a damping factor signifying the loss of nuclear spin alignment arising from dynamic fluctuations of electronic spin and/or inhomogeneous distribution in the local environment.  $\phi$  represents the phase angle introduced due to the finite bending of the incoming beam because of the applied magnetic field. More details of  $G_2(t)$  are given in reference [29].

Figures 3 and 4 compile the observed isomeric states in even-A and odd-A isotopes, respectively, for  $^{128-139}\text{La}$ . The isomers in  $^{135, 136}\text{La}$  [15, 16] isotopes in this region have also attracted a lot of attention. However, the data on moment measurements are very limited. The lighter lanthanum isotopes have been studied with fusion evaporation reaction [9, 31], whereas the heavier isotopes have been produced mainly utilizing fusion–fission [11] and light ion induced reactions [32]. The data on excited states and isomers of  $^{138}\text{La}$  have been rather scarce. It is interesting to see how the measurement of lifetimes and electromagnetic moments of excited states in lanthanum isotopes provide new nuclear structure information such as the configurations of isomeric states, and their comparison with the nuclear model calculations. The analysis of the structure of these isomers is now possible due to the advancement of the large-scale shell model calculations [6]. The measurement of the nuclear moment along with the transition probabilities, enables the investigation of the structure of different isomeric states in  $^{133, 135}\text{La}$  near the  $N = 82$  shell closure and of the hyperfine interaction of La in Fe host. It also allows the testing of all the parts of the effective interaction in odd–odd  $^{138}\text{La}$  ( $Z = 57$  and  $N = 81$ ) nucleus which has neutron holes in the presence of a few proton particles, within the framework of nuclear shell model.

### 2.2.1 The structure of the $11/2^-$ isomeric state in $^{133}\text{La}$

The  $11/2^-$  isomeric state at 535 keV was populated and studied using the reaction  $^{126}\text{Te}(^{11}\text{B}, 4n)^{135}\text{La}$  at beam energy of 52 MeV produced by the PLF at TIFR, Mumbai. The results from this work were reported by Laskar et al. [33]. In this experiment,  $^{126}\text{Te}$  target matrix was thick enough to stop the  $^{133}\text{La}$  ( $Z = 57$ ,  $N = 76$ ) nuclei. The Te metal having a hexagonal close-packed (hcp) crystal structure, produced a non-zero electric field gradient at the probe site. Thus, the  $^{133}\text{La}$  nuclei in the Te host experienced the combined influence of the magnetic dipole and electric quadrupole interaction [34]. Figure 5 shows the lifetime spectrum fitted with an exponential decay curve with energy gate on the 477-keV  $\gamma$  ray transition to give a lifetime ( $T_{1/2}$ ) of  $68.01 \pm 0.41$  ns, with the quoted uncertainty being only statistical; this value is within the range of the previously reported values [9, 35].

The spin-rotation spectrum shows strong damping with a very large value of  $\lambda$  due to the combined effect of the perturbations. A fit of the  $R(t)$  spectrum, as shown in Fig. 6, yielded  $\omega_L = 111.4 \pm 6.7$  Mrad/s and  $\omega_Q = 8.0 \pm 1.0$  Mrad/s. From the  $\omega_L$  value,  $g = 1.16 \pm 0.07$  was extracted, which was found to be close to the value estimated with pure magnetic interaction i.e.  $1.19 \pm 0.06$ . For the determination of the spectroscopic quadrupole moment  $-Q$  from  $\omega_Q$ , the value of the EFG at a lanthanum nucleus site in a  $^{126}\text{Te}$  crystal is required.

From the calculation of density functional theory [36], using the augmented plane wave+local orbital (APW+lo) method [37] as implemented in the WIEN2K package [38], the EFG for the La impurity in Te host has been obtained as  $V_{zz} = 6.7 \times 10^{17}$  V/cm<sup>2</sup> after considering lattice relaxation. Using this value of  $V_{zz}$ , and the expression [34],  $\hbar|\omega_Q| = \frac{eQV_{zz}}{4I(2I-1)}$ , the spectroscopic quadrupole moment of  $11/2^-$  isomer has been extracted as  $|Q| = 1.71 \pm$

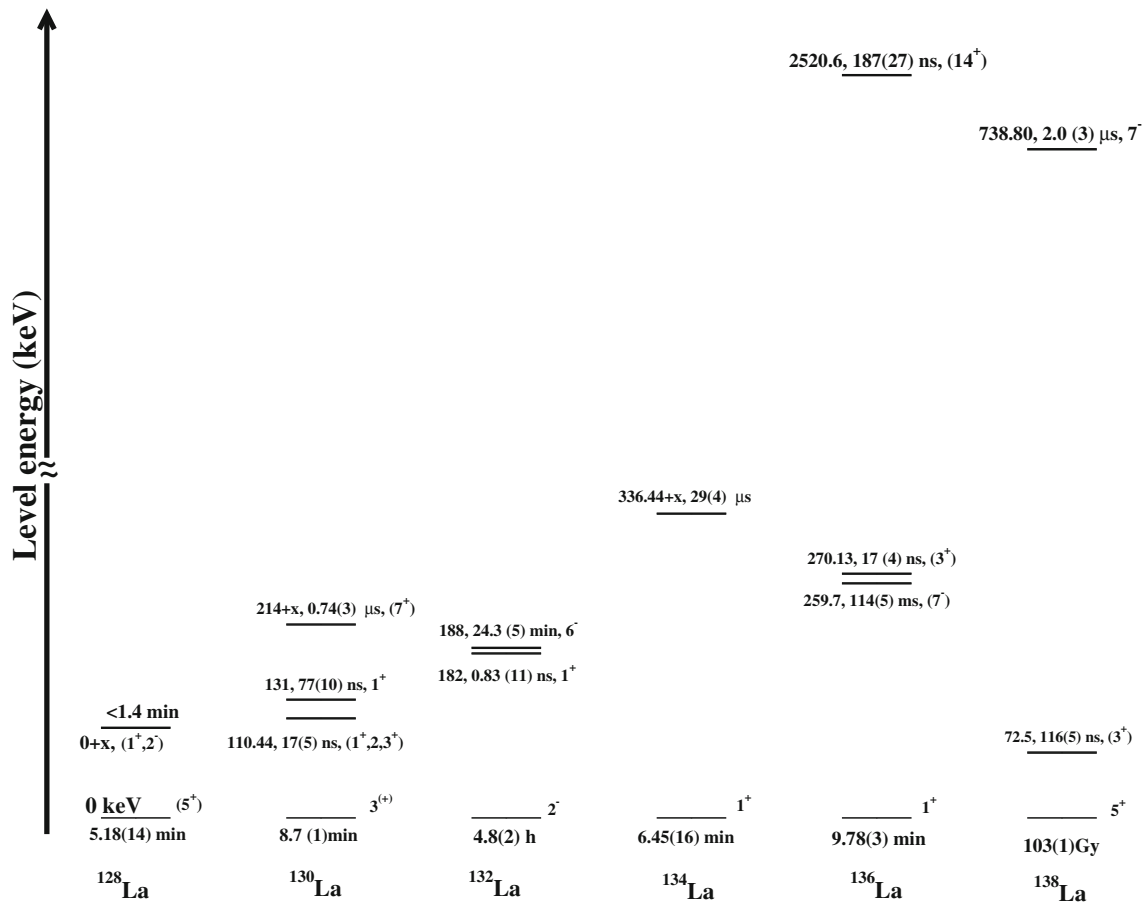


**Fig. 3** A comparison of the experimental excitation energies of isomeric states in odd–odd La isotopes [2, 30]. For the excitation energy, an axis break has been introduced to show the higher energy isomeric states along with lower energy states

0.34 b. The quadrupole moment is related to the deformation parameter  $\beta$ , through the relation

$$Q_s = \frac{3}{\sqrt{5}\pi} eZ\beta(1 + 0.16\beta)R_0^2 A^{2/3} \frac{3K^2 - I(I + 1)}{(I + 1)(2I + 3)} \tag{4}$$

where  $Z$  is the atomic number of the nucleus,  $K$  is the projection of total angular momentum or spin on the symmetry axis,  $I$  is the nuclear spin, and  $R_0 = 1.21$  fm [39, 40]. The value of the deformation parameter was extracted to be  $\beta = 0.28 \pm 0.10$  using  $K = 1/2$  from the Nilsson diagram [33].

### 2.2.2 $g$ -factor measurement of the 2738 keV isomer in $^{135}\text{La}$

The isomer at 2738 keV in  $^{135}\text{La}$  ( $Z = 57, N = 78$ ) was populated and studied using the reaction  $^{128}\text{Te}(^{11}\text{B}, 4n)^{135}\text{La}$ . The 52 MeV pulsed  $^{11}\text{B}$  beam was provided by the heavy-ion accelerator facility at TIFR, Mumbai. An isotopically enriched  $1\text{ mg/cm}^2$   $^{128}\text{Te}$  target evaporated on  $3.5\text{ mg/cm}^2$  Au backing was used. The lifetime of the isomer was remeasured as  $25.3(3)$  ns and reported in Ref. [41]. The experimental modulation ratio  $R(t)$  was formed using the time spectra generated with 471- and 376-keV transitions. The spectra fitted to the Eq. (2) yielded  $\omega_L = 11.30(1.13)$  Mrad/s and  $12.4(1.2)$  Mrad/s for 471- and 376-keV transitions, respectively. These provide the  $g$ -factor of the  $(23/2^+)$  isomeric state in  $^{135}\text{La}$  as  $-0.047(4)$  and  $-0.052(5)$  using  $\omega_L = gB\mu_N/\hbar$  relation, giving a mean value of  $-0.049(3)$ .

The magnetic hyperfine field of La impurity in ferromagnetic Fe host has also been measured by Laskar et al. with TDPAD technique using the precise value of  $g$ -factor of  $23/2^+$  isomeric state in  $^{135}\text{La}$  as a nuclear probe, populated in the reaction  $^{128}\text{Te}(^{11}\text{B}, 4n)^{135}\text{La}$  at beam energy of 52 MeV using  $0.7\text{ mg/cm}^2$  of  $^{128}\text{Te}$  as target evaporated on a thin ( $3\text{ mg/cm}^2$ ) Fe foil, which served as the stopper for the recoiling  $^{135}\text{La}$  probe atoms. Using the relation  $\hbar\omega_L = g_N\mu_N \times B_{\text{eff}}$ , the effective magnetic field  $B_{\text{eff}} (= B_{\text{app}} + B_{\text{hf}})$  was obtained to be  $-40.1 \pm 3.3$  T.

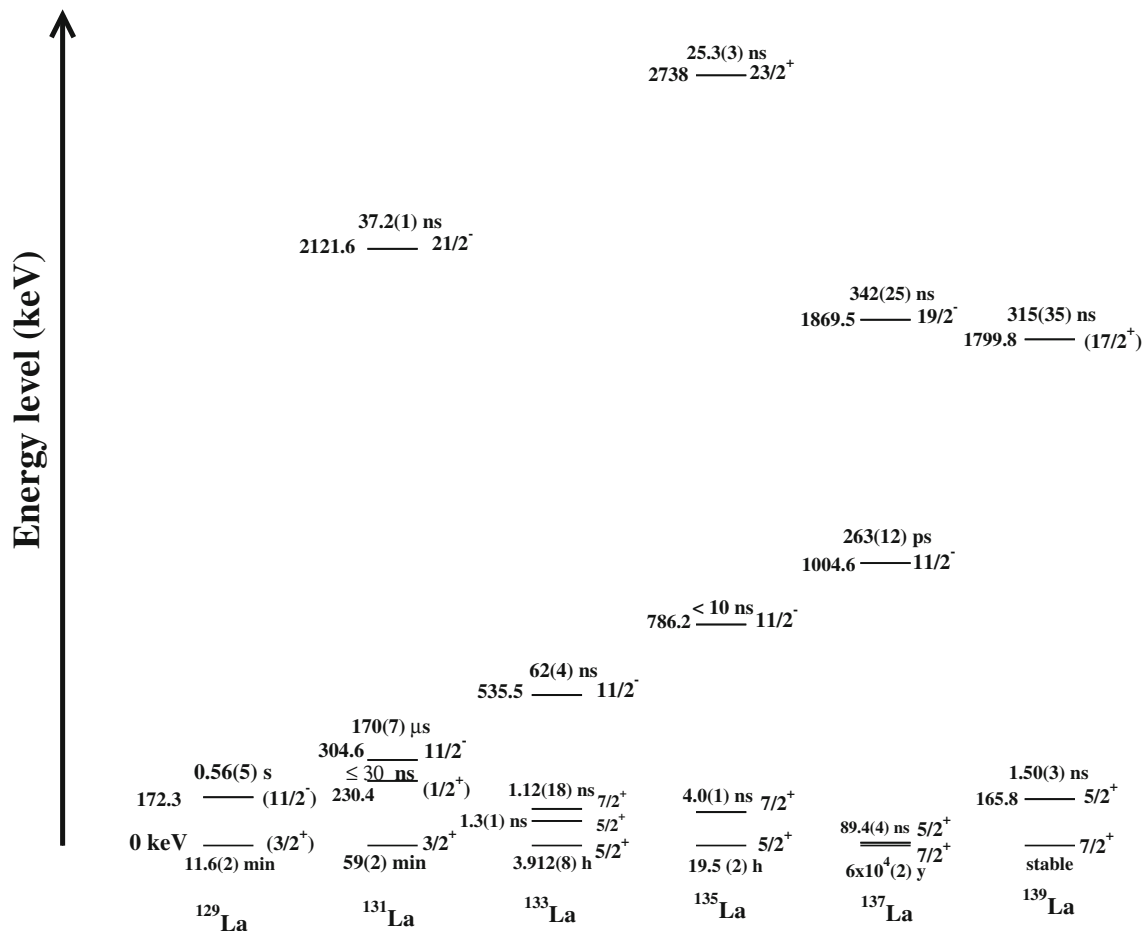
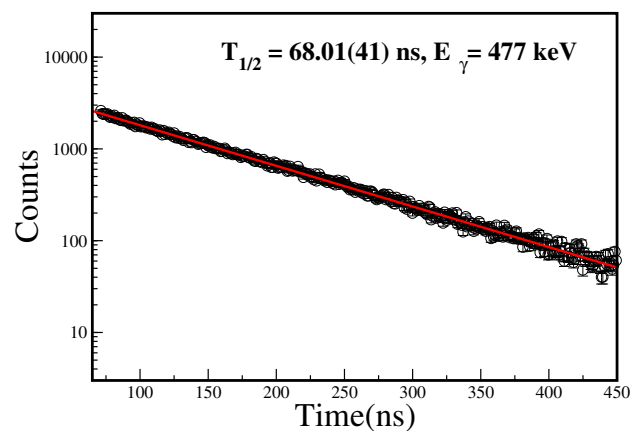


**Fig. 4** A comparison of the experimental excitation energies of isomeric states in odd–even La isotopes [2, 30]

**Fig. 5** Decay curve for the 477 keV  $\gamma$ -ray (taken from Ref. [33])

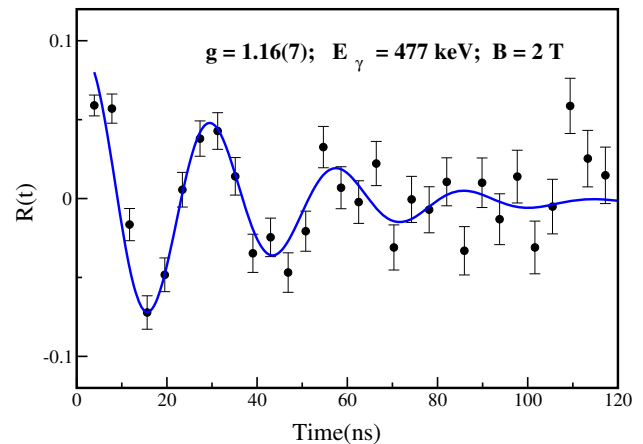


Here,  $B_{\text{app}}$  refers to the applied magnetic field and  $B_{\text{hf}}$  is the hyperfine field at the nuclear site of the La impurity atom. The external applied magnetic field was  $B_{\text{app}} = 2T$ . So the  $B_{\text{hf}}$  was estimated to be  $-42.1 \pm 3.3T$  [42].

### 3 Review of isomeric states in even–even Ba and Ce nuclei

Having discussed the experimental details and the findings related to the isomeric states in odd- $Z$  La isotopes, it should be intriguing to carry out an extensive survey on the even–even neighboring counterparts. This should

**Fig. 6** Spin rotation spectrum at  $B_{\text{ext}} = 2$  T for the  $11/2^-$  isomeric state of  $^{133}\text{La}$  (taken from Ref. [33])



enable one to build up an understanding of the various effects caused by the coupling of single-particle (hole) with an even–even core. The isotopes in Ba and Ce nuclei provide a vast reservoir of different types of isomeric states, however, there are only a few isomeric states which have been reported across all the known isotopes of the said nuclei. Thus, these states equip us with an opportunity to study the variation of their excitation energies, half-lives,  $g$ -factors if available, etc. across the isotopic, isotonic, or isobaric chains. Such studies should be helpful in extracting the underlying physical causes and thus, can be instrumental in revealing mysteries of the evolution of nuclear structure.

In this section, we only concentrate on the existence of a few types of isomers in the mentioned nuclei and discuss some of the physical aspects that will build the platform to enhance our understanding of other nuclei which can be treated simply as odd-particle coupling of either type of nucleon with these even–even core nuclei.

### 3.1 $K$ isomers

The isomeric states that evolve due to the hindrances related to large variations in the total angular momentum projections of axially symmetric deformed states are termed as  $K$  isomers. The decay modes of  $K$  isomers demand extensive probing and are yet to be adequately understood. The first one, out of the three possible decay mechanisms suggested for such decays, involves Coriolis mixing of states with different  $K$  values [43–45] and is generally denoted as  $K$  mixing.

Second, for high- $K$  states, the projection of angular momentum is large along the symmetry axis of the deformed nucleus, whereas, the alignment is along the rotation axis in the yrast band. Therefore, large changes in the orientation can describe the decay modes involving large  $K$  differences [46–48].

The third and the most interesting explanation is based on the assumption of a tunneling motion in the  $\gamma$ -deformation degree of freedom [49–51]. The deexcitation of high- $K$  isomers to  $K = 0$  bands is described through  $\gamma$  tunneling mediated by a barrier that separates the deformation-aligned isomeric states at  $\gamma = -120^\circ$  from the rotation-aligned  $K = 0$  states at  $\gamma = 0^\circ$ . This involves the triaxial shape degree of freedom, although the nucleus is axially symmetric in the initial and final states. Mostly, the  $\gamma$ -soft nuclei are prone to this mechanism [52, 53]. For instance, a second fragmented decay path out of the  $I^\pi = 8^-$  isomeric state of the  $\gamma$ -vibrational band parallel to the ground-state band was identified in  $^{132}\text{Ce}$  [54], that was correlated to an element of triaxial deformation and an appreciable amount of  $\gamma$ -softness. This establishes that  $^{132}\text{Ce}$  is susceptible to  $\gamma$  vibrations which further justifies the results of PES calculations which predict a substantial amount of the  $\gamma$ -deformation around  $\gamma \approx 15^\circ$  [55]. Similar isomeric state was also observed in  $^{138}\text{Gd}$  where Proctor et al., predicted a decreasing trend in  $\gamma$  deformation using the PES calculations for the lower-mass  $K = 8^-$  isomeric states. They suggested that the reduced hindrance could increase with decreasing  $Z$  [56].

In all the even–even  $N = 74$  isotones with atomic number  $Z = 54–64$ ,  $I^\pi = 8^-$  isomers with  $K = 8$  have been observed. The half-lives of these isomers vary by six orders of magnitude, from nanoseconds in Xe, to milliseconds in Ce and Ba. Examples can be found in  $^{130}\text{Ba}$ ,  $^{134}\text{Nd}$ ,  $^{136}\text{Sm}$ , and  $^{138}\text{Gd}$  [43, 57–59]. These isomers are at similar excitation energies changing smoothly from about 2.8 MeV in  $^{128}\text{Xe}$  to about 2.2 MeV in  $^{138}\text{Gd}$  (see Fig. 5 in Ref. [54]). A two-quasineutron configuration based on  $7/2^+[404] \otimes 9/2^- [514]$  is suggested for these isomers.

On the other hand, the  $K$  isomeric state in  $^{130}\text{Ce}$  has been reported to be a  $7^-$  state. The 2454 keV isomeric state has been described by a prolate two-neutron configuration involving the  $7/2^+[404]$  and  $7/2^- [523]$  orbitals coupled with  $K = 7$  [60]. The high- $K$  isomeric states known in the  $N = 72$  isotones  $^{126}\text{Xe}$ ,  $^{128}\text{Ba}$ , and  $^{130}\text{Ce}$ , have different decay modes via  $E1$  transitions to states of the ground state band [60–62]. The potential energy surface calculations performed by Liu et al. [63] concluded that the isomeric state is remarkably soft in the  $\gamma$

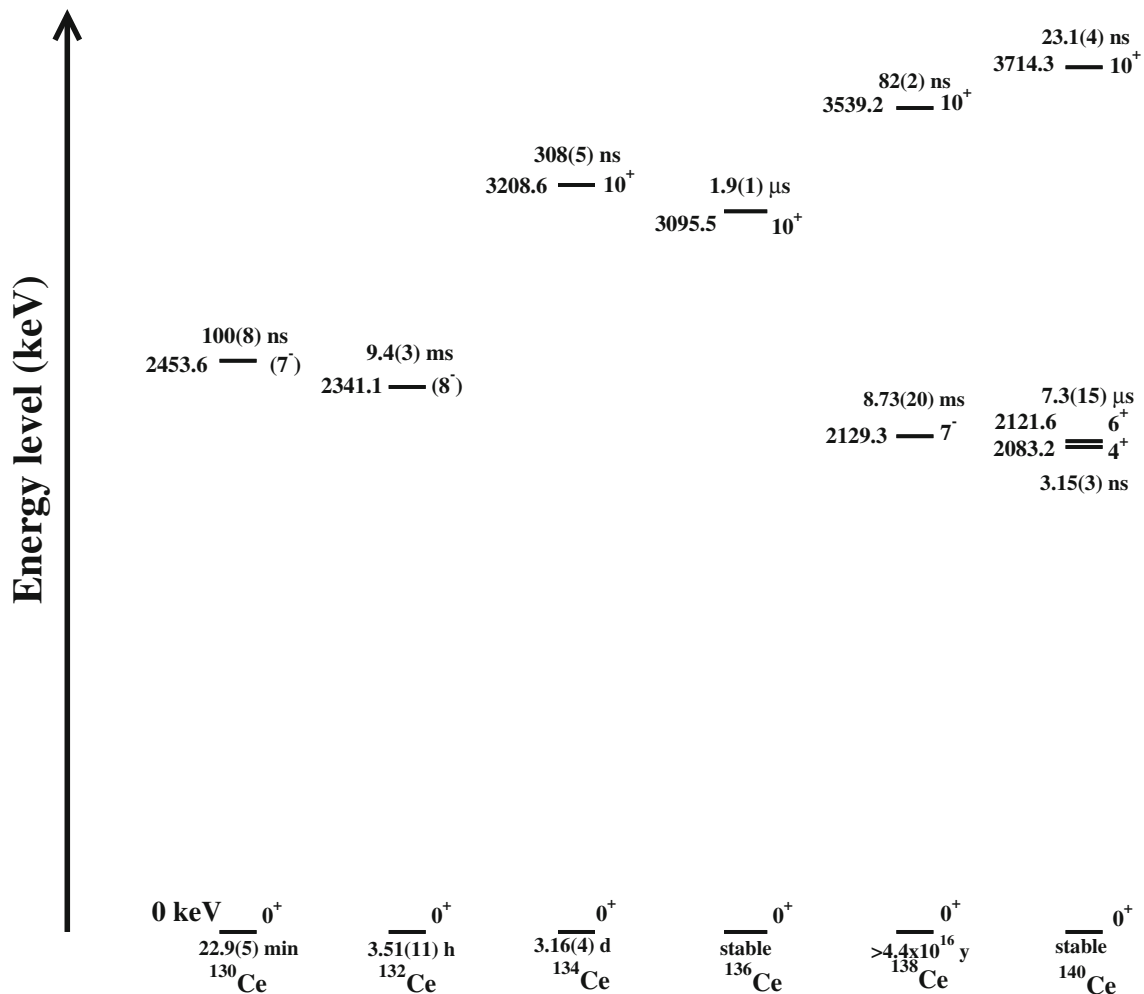


**Fig. 7** The systematic of the experimental excitation energies of isomeric states in even- $A$  Ce isotopes [2, 30]

degree of freedom, which should form the benchmark for the  $K$  mixing. The authors further presented a detailed review on the comparison of the triaxiality of high- $K$  isomers in  $A \sim 130$  regions [64]. The PES results are further consolidated as the observed quadrupole moments could be satisfactorily reproduced. The authors highlighted the observed irregularity in  $Z = 56$  isotonic partner of  $^{132}\text{Ce}$  in terms of a decrease in the hindrance factor  $f_\nu$ , as well as the  $\gamma$  softness from  $^{130}\text{Ba}$  [65] to  $^{132}\text{Ce}$  under the circumstance that both the nuclei have almost the same  $\gamma$  deformations. According to the authors, this behaviour could be related to the shape isomerism for the nuclei approaching the  $Z = 50$  shell closure [53]. This is again in contrast to the  $N = 74$  isotones, where the  $f_\nu$  value increases fast from  $^{128}\text{Ba}$  [66] to  $^{130}\text{Ce}$  in the absence of no obvious shape polarization.

A systematic of isomeric states across even- $A$  Ce isotopes have been displayed in Fig. 7. These states have comparable excitation energy across different nuclei. Interestingly, the occurrence of either 7<sup>-</sup> or 8<sup>-</sup> states is not so frequent beyond  $N = 74$ .

### 3.2 Evolution of $I^\pi = 10^+$ isomers for $N = 76$ onward

As we move from  $^{134}\text{Ce}$  to  $^{138}\text{Ce}$  [67], an isomeric state at  $I^\pi = 10^+$  is consistently observed throughout the isotopic chain. This is very similar to the observation of a similar isomeric state for  $Z = 56$  isotopic chains as well [68, 69] (see Fig. 8). Further, these can also be observed in  $^{144}\text{Gd}$  [70],  $^{140}\text{Sm}$  [71] isotopes. From the measured quadrupole moments, the states can be inferred to be fairly deformed. Moreover, the excitation energy of the state monotonically increases with the increase in the number of neutrons. On the other hand, the half-lives of such states show a decline as a function of neutron number, with  $^{136}\text{Ce}$  being an exception (see Fig. 7). With a motivation to measure directly the sign of the deformation, Dafni et al. has applied the tilted multifoil-TDPAD technique on  $^{134}\text{Ce}(10^+)$  and  $^{138}\text{Ce}(10^+)$  states [72]. It was concluded that positive quadrupole moments should hint towards the occurrence of isomers based on neutron hole configuration in the  $N < 82$  region. The nucleus  $^{134}\text{Ce}$  exhibits strong



backbending above the observed  $8^+$  state. The strong backbending should be dictated by valence  $h_{11/2}$  neutrons as evident from the negative  $g$ -factor recently found for the  $10^+$  state at the backbending [73, 74]. The two  $10^+$  states at excitation energies of 3719.3 and 3208.5 keV in  $^{134}\text{Ce}$  attracted lot of attention. The  $g$ -factor measurements in  $^{134}\text{Ce}$  for these two  $I^\pi = 10^+$  states, lying within a range of  $\approx 500$  keV in excitation energy, suggested that both these states are having a neutron character [75]. Since, the lowest-lying two 2-qp states should usually belong to 2-quasineutron and 2-quasiproton states, the observation of two closed spaced  $10^+$  states with same neutron character is a challenge for nuclear models. It is important to note that the Triaxial Projected Shell Model (TPSM) could explain these observations [76]. In this model, the same 2-quasineutron configuration provides the microscopic structure of the lowest two  $I^\pi = 10^+$  states and sheds new light on the observation of negative  $g$ -factors for the two states. It is important to note that the  $\gamma$ -band built on the 2-quasineutron configuration has modified the band-crossing features in these nuclei giving the lowest two  $I^\pi = 10^+$  states with neutron character [76].

Evidence on the possible contribution of neutron orbitals in the formation of  $10^+$  isomer is seen through the study  $N = 78$   $^{136}\text{Ce}$  nucleus where the state was suggested to be an outcome of contributions either from  $h_{11/2}$  -protons or neutrons. Müller et al. [77] observed that the excitation energies of these  $10^+$  isomers in  $N = 78$  isotones with  $^{136}\text{Ce}$ ,  $^{138}\text{Nd}$  and  $^{140}\text{Sm}$ , agree within 75 keV and, therefore, indicates that the level structure does not change very much with proton number. This hints towards the dominant contribution originating from the neutron orbitals. In addition, the half-life of the  $I^\pi = 10^+$  state in  $^{134}\text{Ba}$  was measured as 2.63(14)  $\mu\text{s}$  [78, 79]. In fact, the experimental magnetic moment of this state ( $\mu = -2.0(1)\mu_N$ ) confirms its neutron character. Extending the discussion to  $^{138}\text{Ce}$  which is  $N = 80$  counterpart of  $^{144}\text{Gd}$ , where an isomeric state at  $10^+$  is also observed [80]. The excitation energies of the  $10^+$  isomeric states in  $^{144}\text{Gd}$  and  $^{138}\text{Ce}$  are similar [81]. The fact, that the excitation energy has a very slow variation with changing proton numbers, indicates that the  $10^+$  states observed in the two  $N = 80$  isotones are based on neutron configuration. The  $10^+$  isomer in  $^{144}\text{Gd}$  decays by strong  $E1$ /weak  $M2$  transitions. On the other hand, in  $^{138}\text{Ce}$ , the  $10^+$  isomer decays by a hindered transition to  $I^\pi = 8^+$  through  $E2$  transition only. The measured half-life of the  $10^+$  isomer in  $^{136}\text{Ba}$  was reported as 94(10) ns giving  $B(E2) = 0.96(10)e^2fm^4$  for the  $10^+ \rightarrow 8^+$  transition. The different characters of the wave functions for the  $10^+$  and  $8^+$  states obtained from the shell model calculations explains the hindrance for the isomeric transition in  $^{136}\text{Ba}$  [69]. The scenario changes for  $^{140}\text{Ce}$  where the  $10^+$  isomer was proposed to be formed due to the four proton configuration  $\pi(1g_{7/2}^2, 2d_{5/2}^2)$  based on the  $g$ -factor measurement [82]. They proposed that the configuration may be the outcome of small admixtures of configurations that contain the outer subshell excitations  $\pi 2f_{7/2}$  and  $\pi 1h_{9/2}$ . Such understanding can further be extended to similar  $E1$  transitions experimentally observed in the  $N = 82$  nuclei  $^{141}\text{Pr}$  [83] and  $^{145}\text{Eu}$  [82].

## 4 Evolution of isomers through the coupling of the odd nucleon with the neighboring even–even core nucleus

In the last section, various aspects of isomeric states in even–even Ba ( $Z = 56$ ) and Ce ( $Z = 58$ ) isotopes have been accessed. In Sect. 2, details of state-of-art experimental methods have been discussed to measure the lifetimes and  $g$ -factors of  $11/2^-$  and  $23/2^+$  isomeric states in odd-mass La ( $Z = 57$ ). Thus, observations in said La isotopes should facilitate understanding of the explicit single-particle contributions towards excitation energy, electromagnetic moments, transition probabilities,  $K$  forbidden, and alignment effects of proton(hole). Then it becomes obvious to survey odd- $A$  Ba and Ce isotopes to unveil the neutron single-particle effects as well. Therefore, it is immensely important to probe into the systematic of the adjacent neighboring odd- $A$  isotopes in La, Ba, and Ce, respectively. The systematic in odd- $A$  nuclei will be further categorized separately for neutron and proton coupling, respectively.

### 4.1 Coupling of odd neutron (hole) and the evolution of isomers in odd mass Ba and Ce isotopes

A systematic study of the isomeric states in the odd- $A$  Ba isotopes has been carried out to understand the effect of the coupling of an odd-neutron to the even–even Ba isotopes. Figure 9 shows the excitation energies and lifetimes of all the observed isomeric states in odd- $A$  Ba isotopes for  $N = 71$  to  $N = 81$ . The  $9/2^-$  state in isomeric odd- $A$  Ba isotopes for  $N = 73, 75$  [84] decays to the  $7/2^+$  state by  $E1$  transition. In  $^{129}\text{Ba}$  nucleus, the low-energy level structure is explained qualitatively based on the coupling of odd neutrons to the even–even  $^{128}\text{Ba}$  triaxial core [85]. Kaur et al. discussed the observed  $g$ -factor of  $-0.192(6)$  to be the confirmation for the  $\nu h_{11/2}9/2^-$  [514] configuration of the  $9/2^-$  isomeric state [85]. This is also in agreement with the  $g$ -factor values of the similar isomeric states in other  $N = 73$  isotones and the neighboring Ba nuclei. Moreover, the authors have also emphasized  $K$ -mixing in  $^{129}\text{Ba}$  in analogy to  $^{130}\text{Ce}$ .

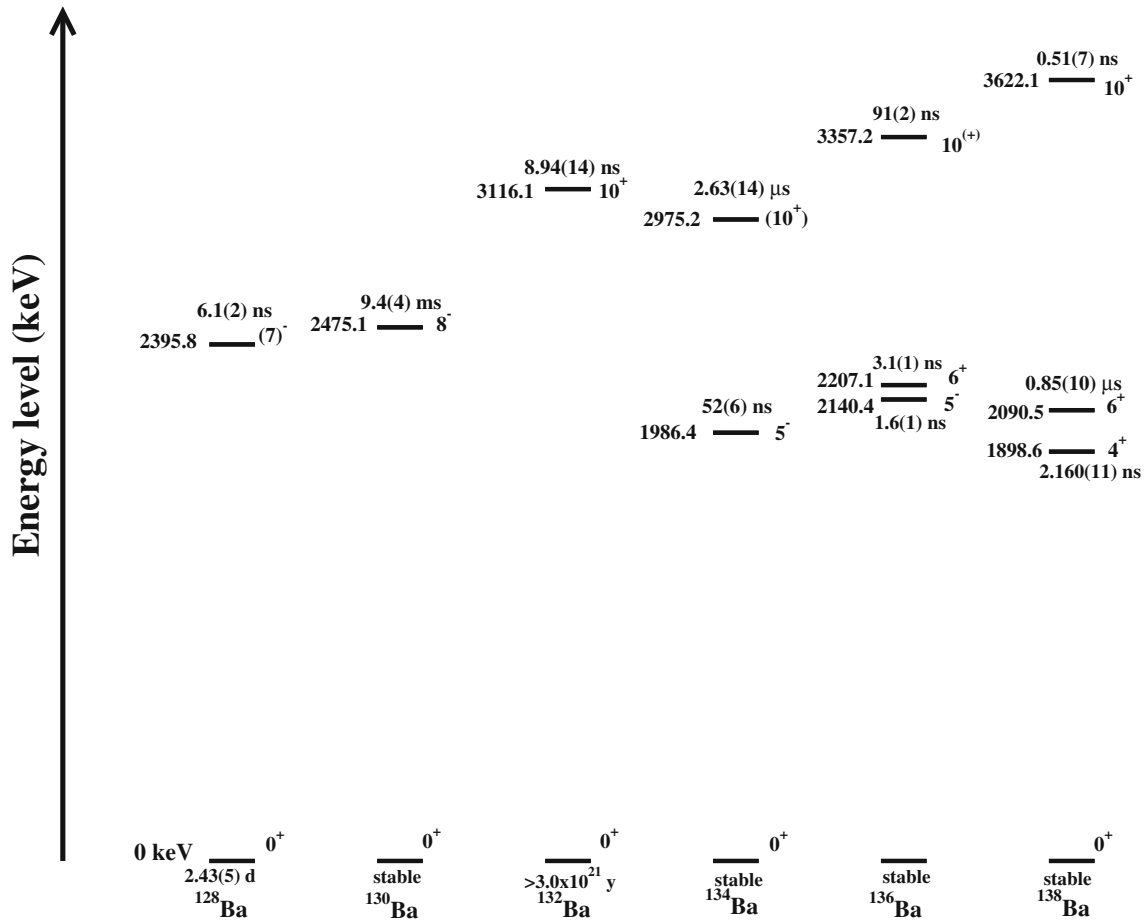
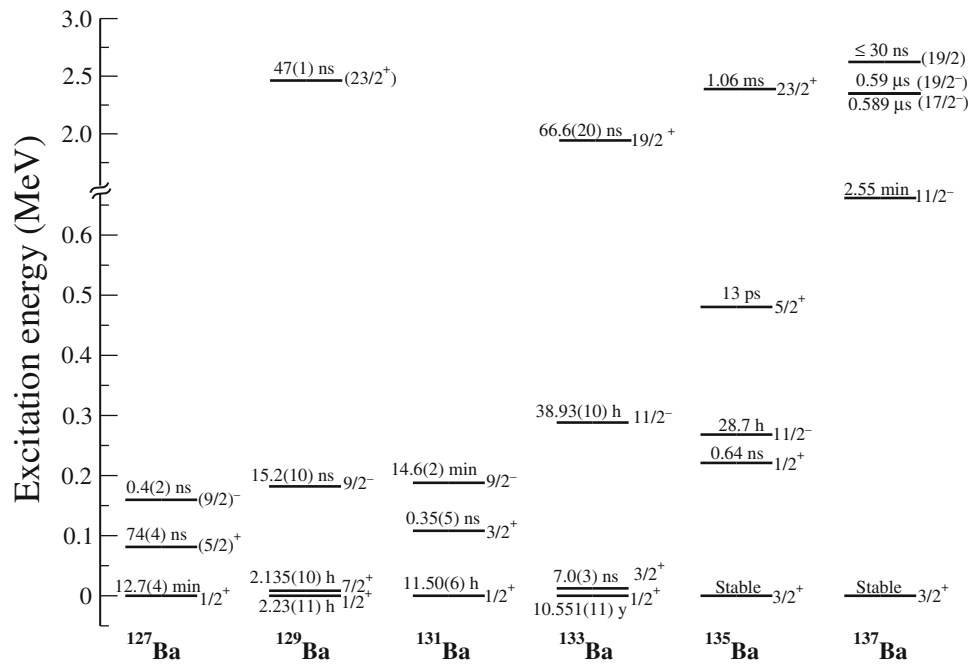


**Fig. 8** The systematic of the experimental excitation energies of isomeric states in even- $A$  Ba isotopes [2, 30]

It should be reiterated that in even–even Ce isotopes, the  $K$ -isomers were observed till  $N = 74$  while isomers based on nucleonic alignment become dominant thereafter. Along a similar line of observation, the  $11/2^-$  state in  $N = 77 - 81$  Ba isotopes with excitation energies 288.2 and 661.6 keV, respectively, [84, 86, 87], evolves as an isomeric state and decays by strong  $M4$  and weak  $E5$  transitions. While for  $^{135}\text{Ba}$  ( $N = 79$ ), no weak  $E1$  branch has been observed for the decay of the  $11/2^-$  state. Hill et al. [88] reported about 38.9 h isomeric state in  $^{133}\text{Ba}$  which was reinvestigated by Thun et al. [89]. In addition, along with the theoretical description of the  $11/2^-$  state in the framework of triaxial rotor-plus-particle model, the first reports on the cascade of states above the  $I^\pi = 11/2^-$  isomer were presented by Gizon et al. [90], where a delayed  $\gamma$ -ray cascade with energies of 83, 681, and 889 keV deexciting an isomeric state at 1942 keV,  $19/2^-$  was observed. A decreasing trend in the half-life of  $11/2^-$  state as a function of increasing excitation energy across  $^{133-137}\text{Ba}$  isotopes is observed. These isomeric decays, mostly mediated through  $M4$  transitions, are considered to be the manifestation of aligned one-neutron holes in  $h_{11/2}$ . Both the electron conversion and the  $\gamma$ -decay branches having  $M4$  and  $E5$  multiplicities for  $11/2^-$  isomeric decay in  $^{133}\text{Ba}$  were studied by Granholms et al. [91]. Furthermore, the  $11/2^-$  isomer in  $^{133}\text{Ba}$  has a weak decay branch to  $^{133}\text{Cs}$  through electron capture. In Ba isotopes for  $N \geq 77$ , the  $11/2^-$  states are known to have  $\nu(h_{11/2})^{-1}$  configuration. The microscopic quasiparticle-phonon model (MQPM) calculations also affirm the same [92].

In a similar line, various studies of the  $N = 79$  odd- $A$  isotones in  $^{137}\text{Ce}$  [93],  $^{139}\text{Nd}$  [94],  $^{141}\text{Sm}$  [95] and  $^{143}\text{Gd}$  [95] showed sequence of levels making weak collective structures based on the  $11/2^-$  isomer at low-spin from which a prolate–oblate transition in these isotopes can be determined. The  $11/2^-$  isomeric state at 268.2 keV is based on the  $h_{11/2}$  neutron hole coupled to the even–even nuclear core. In addition, the  $15/2^-$  state at 950.5 keV may be assigned  $\nu h_{11/2}^{-1} \otimes 2^+$  multiplet whereas the  $19/2^-$  state at 2002.6 keV may belong to the  $\nu h_{11/2}^{-1} \otimes 4^+$  multiplet. The level family based on  $\nu h_{11/2}^{-1}$  multiplet has been systematically observed in various neighboring isotones such as  $^{137}\text{Ce}$ ,  $^{139}\text{Nd}$ ,  $^{141}\text{Sm}$ , and  $^{143}\text{Gd}$ . Shape transition from prolate to oblate has been a very interesting phenomenon in the  $A \approx 135$  transitional region. Examples can be quoted from the neighboring Ce [93] and Nd [94] isotopes

**Fig. 9** The systematic of the experimental excitation energies for the isomeric states in odd-A Ba isotopes [2, 30]. For the excitation energy, an axis break has been introduced to show the higher energy isomeric states along with lower energy states



between  $N = 77$  and  $N = 79$  where such transitions are reported at low-spin states. It was observed that the sequence of the  $13/2^-$  and  $15/2^-$  levels of the  $\nu h_{11/2}^{-1}$  multiplet is a signature of a prolate or an oblate shape. However, the levels with  $13/2^-$  and  $15/2^-$  have not been regularly observed in all the members of the isotonic chain such as in <sup>135</sup>Ba [86].

The calculations suggested that the hindered  $E5$  transition should be accompanied by a single-particle transition  $h_{11/2} \rightarrow s_{1/2}$  while the  $M4$  transition should be based on the single-particle structure  $h_{11/2} \rightarrow d_{3/2}$ . The suppression of the  $E5$  transition relative to the  $M4$  transition can thus be interpreted as the suppression arising from the higher multipolarity  $\lambda = 5$  of the electric transition [96]. The band based on  $h_{11/2}$  configuration is associated with a large signature splitting of about 300 keV in <sup>133</sup>Ba [97].

In addition to the low and medium spin isomers, several high-spin isomers with  $I^\pi = 19/2^+, 23/2^+, \text{ and } 27/2^-$  above the  $I^\pi = 11/2^-$  states were reported in the literature. These isomers are assigned as high-spin members of the  $\nu(h_{11/2}^{-2}d_{3/2}^{-1})$  and  $\nu(h_{11/2}^{-2})$ , higher seniority multiplets [98]. As an example, the systematic of  $I^\pi = 23/2^+$  states in <sup>129</sup>Sb, <sup>131</sup>I, <sup>133</sup>Cs and <sup>135</sup>La is shown in Fig. 10. The  $23/2^+$  isomers are resulted from the coupling of the  $10^+$  isomer of the even-even isotopes coupled with odd proton. More details are given in the subsection 4.2.1.

Further, a detailed study of isomeric  $I^\pi = 23/2^+$  states was performed in <sup>133</sup>Xe and <sup>135</sup>Ba by Kaya et al. [98]. The  $23/2^+$  isomer is also observed in  $N = 79$ , <sup>135</sup>Ba and the isomer decays by  $M2 + (E3)$  transition. The main configuration of the shell-model  $23/2_1^+$  wave function is  $\nu(h_{11/2}^{-2}d_{3/2}^{-1})$ , i.e. a neutron hole in the  $d_{3/2}$  coupled to the  $10^+$  ( $\nu(h_{11/2}^{-2})$ ) state of <sup>136</sup>Ba. The dominant  $M2$  characters for 231-keV transition in <sup>133</sup>Xe and the 254-keV transition in <sup>135</sup>Ba have been established from the multipole-mixing ratio and internal-conversion coefficient measurements. The experimentally determined  $B(M2)$  and  $B(E3)$  transition strengths when compared to the results of large-scale shell-model calculations produced a good agreement with the experimental findings. In general, no states were reported beyond the  $I^\pi = 23/2^+$  isomers in <sup>135</sup>Ba. Hence, measurements in <sup>135</sup>Ba are of high interest to find structure above this isomer. Interestingly, despite a detailed description of the high-spin regime in <sup>137</sup>Ce, no  $I^\pi = 23/2^+$  isomer has been reported to date. Even the state  $23/2^+$  was tentatively assigned. Therefore, future experiments are desired to elucidate a possible onset of  $I^\pi = 23/2^+$  isomerism in <sup>137</sup>Ce.

It will be interesting to study how the neutron particle couples with the isomeric states in even mass Ce nuclei. In the nuclei <sup>129, 131, 133</sup>Ce, there exist states based on the  $\Omega = 9/2$ . On the other hand, the state with  $\Omega = 11/2$  becomes dominant from <sup>135</sup>Ce onward. Based on the triaxial-rotor-plus-particle model calculations for the bands of <sup>129, 131, 133, 135, 137</sup>Ce nuclei, one finds that the asymmetry parameter  $\gamma$  increases and the deformation parameter  $\beta$  decreases with increasing neutron number [99–101]. For <sup>135</sup>Ce, the  $\gamma$ -deformation approaches  $30^\circ$ . These systematic investigations suggest that a transition from prolate to oblate shape through  $\gamma = 30^\circ$  occurs between <sup>135</sup>Ce and <sup>137</sup>Ce [80].

The upper  $19/2^-$  state in <sup>137</sup>Ce could be derived from the coupling of a  $h_{11/2}$  neutron hole to the  $6^{(+)}$  state in <sup>138</sup>Ce which has been interpreted to be of  $[\pi g_{7/2}]_{6^+}^2$  or  $[\pi g_{7/2}d_{5/2}]_{6^+}$  configuration. The  $21/2^+$  state in <sup>137</sup>Ce

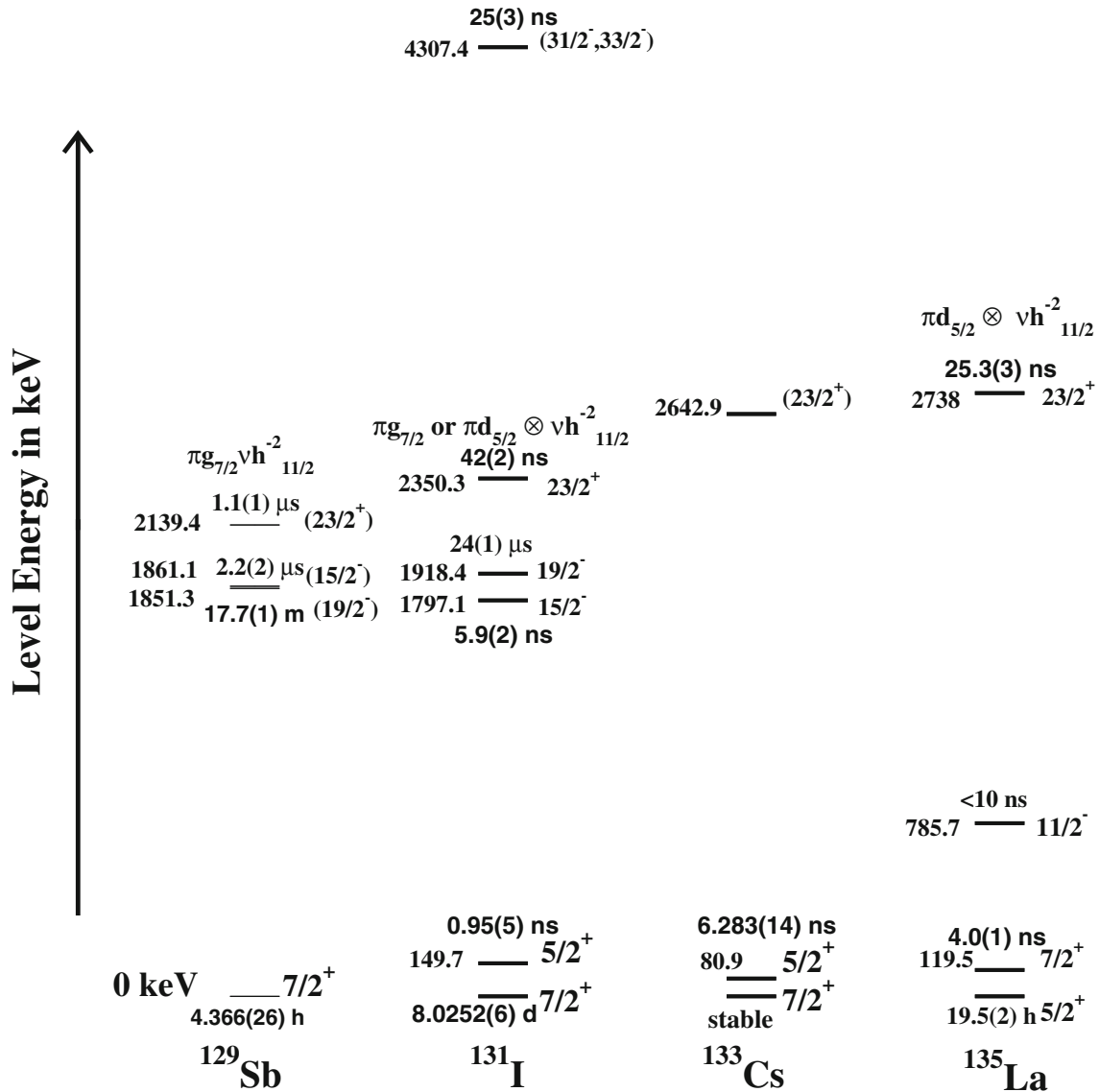


**Fig. 10** The systematic of 23/2<sup>+</sup> isomeric state in N = 78 isotones [2, 30]

has an excitation energy very similar to that of the 5<sup>-</sup> state in <sup>138</sup>Ce. The 21/2<sup>+</sup> state may have a configuration based on the coupling of a h<sub>11/2</sub>, neutron hole to the 5<sup>-</sup> state in the core nucleus <sup>138</sup>Ce.

It is interesting to note that no quadrupole transition has been found on top of the 21/2<sup>(+)</sup> state as has been observed on top of the 19/2<sup>+</sup> isomer in <sup>135</sup>Ce. Assuming that the 21/2<sup>(+)</sup> state results from the coupling of a h<sub>11/2</sub> neutron to the 5<sup>-</sup> in <sup>138</sup>Ce of [ $\nu h_{11/2}^{-1}, d_{3/2}^{-1}$ ]5<sup>-</sup> configuration it has to be concluded that in <sup>137</sup>Ce a coupling mechanism applies which is different from that for the case of 19/2<sup>+</sup> isomer in <sup>135</sup>Ce.

It is to be highlighted that the  $\gamma$  degree of freedom plays an important role in the description of the structure of nuclei in A  $\approx$  135. The neutrons and protons occupying the h<sub>11/2</sub> in the high- $\Omega$  and low- $\Omega$  orbitals, respectively, lead to the occurrence of triaxial shapes, due to their different deformation-driving properties of these orbitals.

Calculations by Ionescu-Bujor et al. [102] for the quadrupole moment for the isomeric bandhead in <sup>131</sup>Ce, suggested its strongly dependence on the  $\epsilon_2$  parameter and weak variation with the triaxiality parameter. In addition, it also depends on the Coriolis interaction strength, however, the ordering of 9/2<sup>-</sup> and 11/2<sup>-</sup> was observed to remain the same with or without Coriolis interaction term for both low and high values of  $\gamma$  deformation parameter. It was also interpreted that the level of excitation energies above the isomeric state have been found to be less sensitive to the quadrupole deformation, but show a marked dependence on the triaxial parameter. The less dominance of the quadrupole deformation factor is also seen in <sup>129</sup>Ce where the hexadecapole—deformation parameter has to be included to reproduce the observed quadrupole moment values. According to PTR model

calculations, the mixing of the intrinsic orbitals from the  $h_{11/2}$  neutron subshell is involved for the structure of isomeric bandheads in  $^{129,131}\text{Ce}$ . The magnetic moments of the isomeric bandheads have small variations with deformation parameters. The reason being that the wave functions contain only contributions from the  $h_{11/2}$  single-particle state. The calculated  $g$ -factors with the adopted parameters were found in good agreement with the measured values. The study indicates the trend of decreasing  $\varepsilon_2$  and increasing  $\gamma$  with the neutron number was also observed in  $^{129,131}\text{Ce}$  nuclei, however, the variations of  $\varepsilon_2$  and  $\gamma$  parameters are more compared to the Xe and Ba chains.

### 4.2 Coupling of odd proton and the evolution of isomers in La isotopes

The theme of this review article revolves around the aspects of isomeric states in odd- $A$  La isotopes and the subsequent correlations with even–even and odd–odd neighbors. A detailed discussion on some of the isomeric states in odd- $A$  La has been provided in section 2. Further, a comprehensive understanding was tried to be built in connection to the even–even counterparts along with the effect of coupling of odd valence neutron to those cores. It is now imperative to complete the discussion by building the understanding of the coupling of odd valence protons to the even–even core and its effects on the isomeric states.

#### 4.2.1 Isomers and high spin structure of La isotopes

We begin our survey with  $^{135}\text{La}$  ( $Z = 57, N = 78$ ). The systematic of the observed isomers in  $N = 78$  were reported in [103–105]. Recently,  $g$ -factor of  $23/2^+$  isomeric state at 2738 keV in  $^{135}\text{La}$  has been measured using the TDPAD technique by Laskar et al. [41]. The motivation was to investigate the level scheme and the structure of the isomeric level microscopically, Large-scale shell-model (LSSM) calculations were performed. A model space consisting of  $0g_{7/2}, 1d_{5/2}, 1d_{3/2}, 2s_{1/2}$ , and  $0h_{11/2}$  single-particle orbits was considered for both protons and neutrons. The effective interaction used was based on SNBG3 interaction for the neutron-neutron interaction, the N82GYM interaction for the proton-proton interaction, and the monopole-based universal interaction for the proton-neutron interaction [41]. The  $M$ -scheme dimension of the LSSM calculations was obtained to be  $3 \times 10^9$ . These calculations were performed with the KSHELL code [6] utilizing the Oakforest-PACS supercomputer.

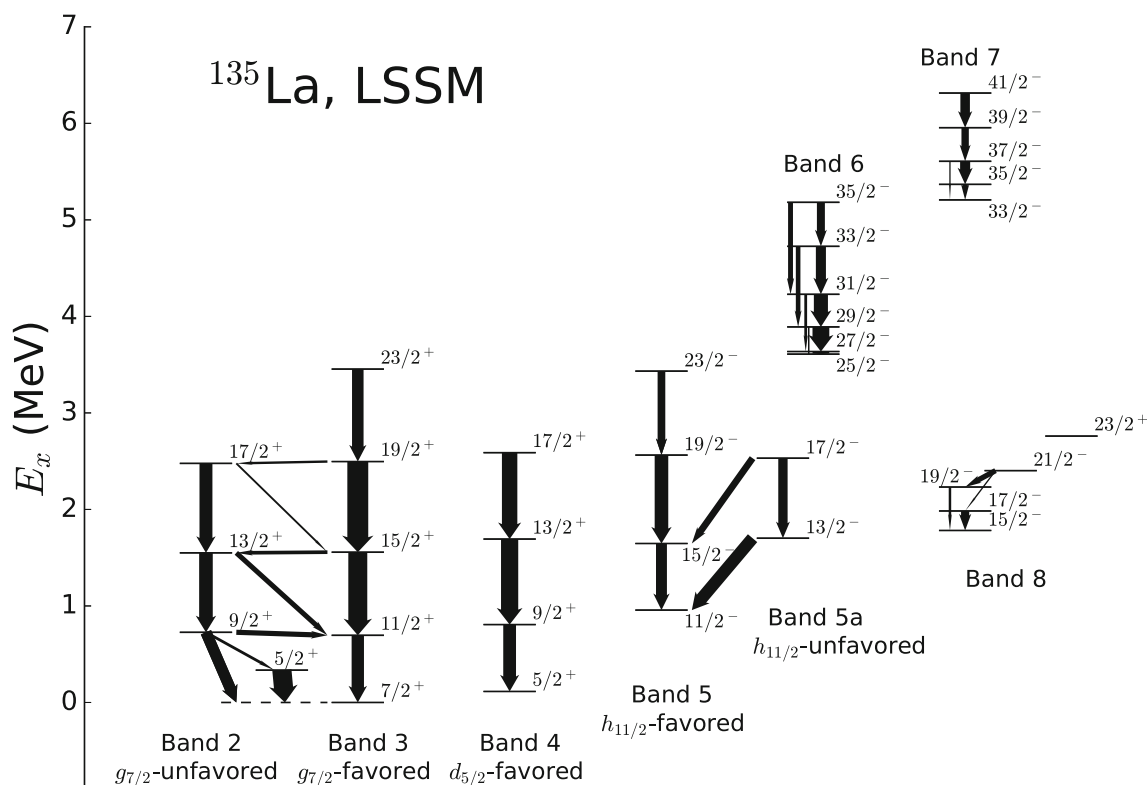


**Fig. 11** Results of the LSSM calculations for the level scheme of  $^{135}\text{La}$  with the SNV interaction (taken from [41]). The arrow width is proportional to the  $B(E2)$  value. The labeling of the bands follows the labels of the experimental bands in Ref. [31]

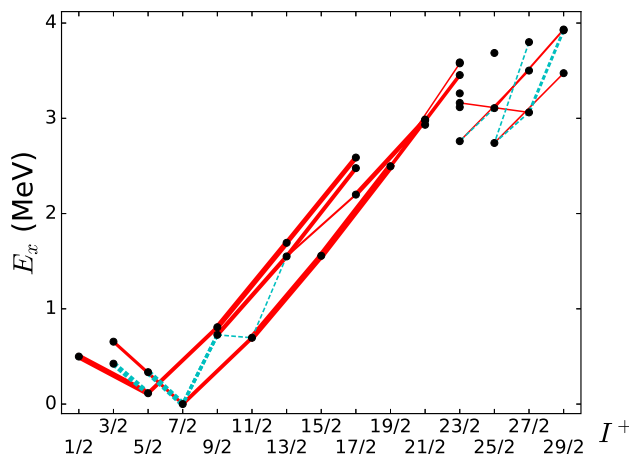


**Fig. 12** LSSM results of excitation energy against the total angular momentum  $I$  for positive-parity states of  $^{135}\text{La}$ . The  $B(E2; I + 2 \rightarrow I)$  and  $B(E2; I + 1 \rightarrow I)$ , are represented by the red solid and cyan dashed lines, respectively. The  $B(E2)$  values larger than  $400 \text{ e}^2\text{fm}^4$  are presented. The thickness of the lines denotes the transition probabilities (taken from Ref. [41])

Figure 11, taken from Fig. 4 in [41], shows the level scheme of  $^{135}\text{La}$  where the arrow width is proportional to the value of  $B(E2)$  transition probabilities of  $^{135}\text{La}$  obtained by the LSSM calculations with the SNV interaction. In this work, the measured excited states have been very well reproduced with the LSSM calculations.

Figure 12, that is Fig. 5 in [41] shows the “ $E2$ -map” [106], which was introduced as a tool to visualize the complex bands connected by the  $E2$  transitions obtained by theoretical calculations. In this plot, the shell-model excitation energy of each positive parity state was plotted as a function of the angular momentum  $I$ . The widths of the connected lines represent the  $B(E2)$  transition probabilities of the respective transitions. Two favored and one unfavored bands, viz. band 2, 3, and 4, respectively, were highlighted by three thick  $B(E2)$  lines in Fig. 11, respectively. According to Laskar et al., the observed  $3/2_1^+$  ( $E_x = 265 \text{ keV}$ ) and  $1/2_1^+$  ( $E_x = 300 \text{ keV}$ ) states [107] most likely correspond to the  $d_{5/2}$  unfavored states shown in Fig. 12. This further strengthens the capability of the present LSSM calculation to describe the complex band structures of  $^{135}\text{La}$ .

In the work by Laskar et al. it was observed that the calculated excitation energy of  $2.760 \text{ MeV}$  for  $23/2^+$  state agrees very well with the experimental value of  $2.738 \text{ MeV}$ . The  $23/2_1^+$  state has no strong decay paths with large  $B(E2)$  values to the other states. This is indicative of the isomeric property of the level. The authors report the shell-model excitation energy of  $21/2_1^+$  to be  $2.932 \text{ MeV}$ , which is higher than  $23/2^+$  ( $2.760 \text{ MeV}$ ) and thereby prohibits the decay to the  $21/2_1^+$  state. The authors noted another  $E2$ -decay possibility through  $264 \text{ keV}$   $\gamma$  transition from  $23/2^+$  to  $19/2^+$  state. The corresponding  $B(E2; 23/2_1^+ \rightarrow 19/2_1^+)$  was measured to be  $0.5 \text{ e}^2\text{fm}^4$ , which is quite small. Its partial half-life was estimated to be  $260 \text{ ns}$  which is many fold longer than the observed lifetime of the isomeric state, i.e.,  $25.3(3) \text{ ns}$ . Such observation justifies the expected  $E1$  decay to the  $21/2_1^-$  state. Hence, the  $23/2_1^+$  was concluded to be the isomeric state.

The calculated four  $23/2^+$  states and their single-particle spectroscopic factors  $C^2S$  by the LSSM were presented by Laskar et al. that is presented in Table 1.

The single-particle spectroscopic factor,  $C^2S$ , is reckoned to be a good measure for describing nuclear structure. From the table, it can be perceived that the  $C^2S$  of  $^{134}\text{Ba}(10^+) \otimes \pi 1d_{5/2} = 23/2_1^+$  stands with the largest value among all other possible couplings. Hence, the major contribution to  $23/2_1^+$  state was concluded to be from  $\pi(d_{5/2}) \otimes \nu(h_{11/2})^{-2}$  configuration in accordance to  $\nu(h_{11/2})^{-2}$  based configuration for the  $10^+$  state of  $^{134}\text{Ba}$ .

**Table 1** LSSM results for the single-particle spectroscopic factors  $C^2S$  to show the decomposition of the four  $23/2^+$  states of  $^{135}\text{La}$  (adopted from [41])

$I^\pi$	Ex (MeV)	$^{134}\text{Ba}(10^+) \otimes \pi 1d_{5/2}$	$^{134}\text{Ba}(10^+) \otimes \pi 0g_{7/2}$	$^{134}\text{Ba}(10^+) \otimes \pi 1d_{3/2}$	$^{134}\text{Ba}(7^-) \otimes \pi 0h_{11/2}$
$23/2_1^+$	2.760	0.479	0.073	0.011	0.000
$23/2_2^+$	3.117	0.027	0.131	0.000	0.000
$23/2_3^+$	3.162	0.004	0.078	0.036	0.006
$23/2_4^+$	3.262	0.000	0.001	0.002	0.593

The study of  $23/2^+$  state highlights the importance of such states in accessing the coupling interaction of a single nucleon with the core. However, other odd-mass La isotopes in this mass region are yet to be probed to observe  $23/2^+$  state and hence it will be too early to comment on the evolution of such state across the isotopic chain in La. On the other hand, a systematic study across the  $N = 78$  isotonic chain was made which provided some interesting results. In Fig. 10, the state  $23/2^+$  is compared across  $^{129}\text{Sb}$  [108],  $^{131}\text{I}$  [109] and  $^{135}\text{La}$ . It is observed that the excitation energy of the state increases as a function of a number of protons, whereas, the half-life of the state decreases. The configuration of the state was described by coupling the  $g_{7/2}$  proton with the two neutron holes in  $h_{11/2}$ . In addition, the isomeric state is also present in  $^{131}\text{Sb}$  with a similar half-life value [110]. It is interesting to observe that most of the other isomers except for the  $23/2^+$  state in  $^{129}\text{Sb}$  are also present in  $^{129}\text{I}$  which happens to be the member of the same isobaric chain. So, the search for  $23/2^+$  isomeric state should be pursued in  $^{129}\text{I}$ . Hence, the existence of high-spin isomers should also be studied as a function of different combinations of a number of protons and neutrons. This will equip us with the understanding of not only the ( $T = 1$ ) nucleons but also with ( $T = 0$ ) nucleon pairs. Biswas et al. [8] reported the high-spin states in  $^{133}\text{Cs}$  where it was seen that the variation of excitation energy across the cascade around the state  $23/2^+$  is quite similar to that observed in the above mentioned nuclei. Further, the shell model results also suggest a similar configuration as reported for the isotonic chain discussed above. Therefore, the existence of isomer at  $23/2\hbar$  cannot be ruled out in  $^{133}\text{Cs}$ .

Many high-spin isomers have been reported in nuclei around  $A \approx 135$  with neutron numbers close to  $N = 82$  shell closure with simple multi-quasiparticle configurations. The lanthanum isotopes are enriched with lots of low- and high-spin isomers, as shown in Figs. 3 and 4. In particular, these isomers will provide insight into the evolution of the nuclear structure of lanthanum isotopes approaching the  $N = 82$  shell closure.

#### 4.2.2 Discussion on $11/2^-$ isomer in odd-A La isotopes

As can be seen from the Fig. 4, the level energy of the  $11/2^-$  isomers in odd mass La nuclei increases and the half lifetime decreases monotonically from  $^{129}\text{La}$  to  $^{137}\text{La}$ . The  $11/2^-$  level is largely  $\pi h_{11/2}$  in nature, i.e; based on proton dependent configuration. The decrease in lifetime with increasing neutron number is a consequence of the hindrances to  $E1$ ,  $M1$ , and  $M2$  transitions and the enhancement of  $E2$  and  $E3$  transitions from the  $11/2^-$  level to the lower positive-parity states. The spectroscopic quadrupole moments and  $g$ -factors of the  $11/2^-$  states in La isotopes are presented in Table 2. Those of the  $^{135,137,139}\text{La}$  are evaluated by the LSSM without any truncation. The effective charges  $(e_p, e_n) = (1.6, 0.8)e$  were used in this calculation. The quadrupole moment of  $^{139}\text{La}$  ( $N = 82$ ) was found to be rather small. However, the quadrupole moment increases gradually as the neutron number decreases indicating an increase in the quadrupole collectivity. The LSSM quadrupole moment of  $^{133}\text{La}$  was obtained as  $Q = -1.25b$  in comparison with the experimental value,  $|Q| = 1.71 \pm 0.34b$ . On the other hand, the  $g$ -factors of the isotopes rather show a constancy that is indicative of a proton  $h_{11/2}$  configuration based structure. Table 2 also shows the single-particle spectroscopic factor  $C^2S$  of the proton  $h_{11/2}$  orbital coupled with the ground states of the corresponding Ba isotopes. As the neutron number increases, a modest increase is observed in  $C^2S$ . The LSSM spectroscopic factor of this isomeric state with the ground state of  $^{132}\text{Ba}$  is  $C^2S = 0.60$ , which is large enough to again support the proton  $h_{11/2}$  configuration.

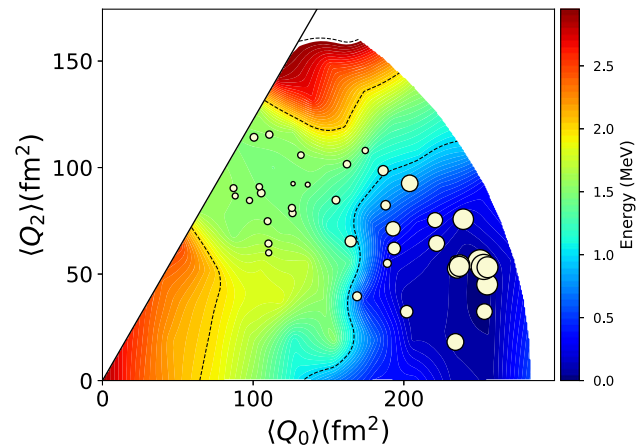
To discuss the intrinsic shape of the  $11/2^-$  state of  $^{133}\text{La}$  in terms of the shell-model framework, Laskar et al. [33] presented the energy surface and the  $T$ -plot of the Monte Carlo shell model (MCSM) calculations [111]. The published figure is reproduced in Fig. 13. In the figure, the contour lines represent the energy surface obtained by the quadrupole-constrained Hartree-Fock method [112] utilizing the same shell-model Hamiltonian. the prolate minimum with modest triaxiality at  $Q_0 = 260 \text{ fm}^2$  is retrieved from the potential energy surfaces, which corresponds

**Table 2** LSSM results on  $g$ -factors, spectroscopic quadrupole moments, and single-particle spectroscopic factor  $C^2S$  of the  $11/2^-$  states of La isotopes

	LSSM $^{139}\text{La}$	$^{137}\text{La}$	$^{135}\text{La}$	$^{133}\text{La}$	Exp. $^{133}\text{La}$
$g$ -factor	1.23	1.20	1.18	1.16	1.16 (7)
$Q$ -moment ( $b$ )	-0.49	-0.80	-1.00	-1.25	1.71 (34)
$C^2S(\pi h_{11/2})$	0.89	0.73	0.68	0.60	

The experimental values reported in Ref. [33] are shown in the rightmost column. Note that the experimental  $Q$ -moment of  $^{133}\text{La}$  is obtained as the absolute value. The  $C^2S$  is obtained by the proton  $h_{11/2}$  attached to the ground state of the neighboring Ba isotopes (adopted from Ref. [33])

**Fig. 13** For the  $11/2_1^-$  state in  $^{133}\text{La}$  the  $T$ -plot, coordinated by the intrinsic mass quadrupole moments,  $Q_0$  and  $Q_2$ . The contour line shows the energy surface obtained by the  $Q$ -constrained Hartree-Fock method with the variation after parity projection. The locations of the circles indicate the intrinsic shape of the MCSM basis states (taken from Ref. [33])



to the deformation parameter  $\beta = 0.16$  (see Fig. 13) [113]. The LSSM value of  $Q = -1.25$  b provides the  $\beta = 0.19$  by using Eq. 4, while assuming  $K = 1/2$ .

In the MCSM framework, it is customary to express the resultant wave function as a superposition of the angular momentum-projected, parity-projected Slater determinants. Each of these form the MCSM basis state. To visualize the intrinsic deformation of the MCSM wave function, the quadrupole deformation of each of the MCSM basis states is represented as a white circular dot in Fig. 13. The area of each dot denotes the overlap between the MCSM basis state and the resultant wave function. The MCSM basis states distribute around the minimum of the energy surface, indicating that the shell-model wave function of the  $11/2_1^-$  state is a prolate shape with a certain shape fluctuation in the  $\gamma$  degrees of freedom.

The lifetime of the  $11/2^-$  state decreases once one moves towards the higher  $A$  La isotopes. This should imply that the  $11/2^-$  state manifests collective properties from  $^{135}\text{La}$  onwards. The reduced transition probability for the 993.7 keV transition in  $^{137}\text{La}$  is found to be  $B(E3) = ((26.0 \pm 2.7) \times 10^3) e^2 \text{ fm}^6$  from lifetime measurement. The value corresponds to  $23.3 \pm 2.4$  W.u. in Weisskopf single-particle estimate. The  $E3$  enhancement of the  $11/2^-$  to  $5/2^+$  transition in the lighter odd- $A$  La isotopes has been suggested to be due to the participation of the octupole vibrations [22]. The change in the  $E3$  transition rate can be attributed to the changing nature of the  $5/2^+$  level, i.e., the contribution of the  $2d_{5/2}$  to the  $5/2^+$ . However, this trend is very similar to that of decreasing half-life of  $11/2^-$  state as a function of increasing excitation energy across  $^{133-137}\text{Ba}$  isotopes. These isomeric decays are mostly mediated through  $M4$  transitions and are manifestations of aligned one-neutron holes in  $h_{11/2}$ . On the other hand, even though, the neutron-aligned  $11/2^-$  isomeric state rises in excitation energy across  $\sim ^{135-139}\text{Ce}$ , the half-lives do not show a particular trend. Coupling of the many-particle configurations to the octupole vibration can be very astonishing. The favored configurations are often those which are related by a spin/parity difference of  $3^-$ , leading to strong  $E3$  transitions and hence isomers based on the high-multipole order in the formation of the yrast line.

Laskar et al. [22] highlighted the importance of  $g$ -factor measurements in explaining the single-particle coupling with the even-even core. The authors compared and showed that measured  $[B(E3); 11/2^- \rightarrow 5/2^+]$  values in  $^{137}\text{La}$  is larger than that of the lighter odd- $A$  La isotopes. However, this is comparable with the  $[B(E3); 3^- \rightarrow 0^+]$  in  $^{136}\text{Ba}$ , which is an isotone of  $^{137}\text{La}$ . On the other hand, the  $B(E3)$  in  $^{133}\text{La}$  is much smaller compared to the  $[B(E3); 3^- \rightarrow 0^+]$  of  $^{132}\text{Ba}$ . The sudden rise of  $B(E3)$  in  $^{137}\text{La}$  was explained using the theoretical calculations of random-phase approximation, where the proton  $g_{9/2}$  orbit was activated by increasing of neutron number occupying  $h_{11/2}$  orbit [22]. On the other hand, such enhancement was not at all seen in Ba isotopes. The study indicated a possible role of the unknown contribution of proton-neutron correlation on the evolution of  $[B(E3); 11/2^- \rightarrow 5/2^+]$  strength in La isotopes which should be scope for future explorations.

Accordingly, the study of such isomeric states which are deemed to be evolved through particle-phonon coupling does show that the nature of octupole collectivity originating through particle-phonon coupling is quite different from the  $B(E3)$  strength in even-even isotones. Thus, it is important to do a systematic study of the existence of isomeric states across the isotopic as well as isotonic chains with an emphasis on understanding the dynamics of the interaction that causes the sudden rise of the proton  $g_{9/2}$  contribution in the transition densities near  $N = 82$ . As an example, the  $N = 76$  isotonic chain was considered to study the systematic of  $11/2^-$  state across different isotones for  $Z = 55, 57, 59$ . The excitation energy of the isomeric level at  $11/2^-$  has been found to be decreasing monotonically as the  $Z$  increases. On the other hand, the lifetime increases as the  $Z$  increases. This highlights that the state should be dominated by the proton contribution from the alignment across  $h_{11/2}$  orbitals. For the odd proton nuclei, the Fermi surface is located just below the states that originate from the  $h_{11/2}$  shell in the



Nilsson scheme. Wisshak et al. [114] implemented an alignment coupling model and concluded that such states should have a prolate shape with low or medium axial deformation. Md. Laskar et al. reported the  $11/2^-$  state in  $^{133}\text{La}$  to be a result of coupling of  $h_{11/2}$  proton with the  $0^+$  state of  $^{132}\text{Ba}$  through  $g$ -factor measurements. It was further argued that the  $11/2^-$  state should be of prolate nature with certain fluctuations in the  $\gamma$ -degree of freedom [33]. A comparison of the measured  $g$ -factor for  $11/2^-$  state in  $^{133}\text{La}$  ( $N = 76$ ) was made with that of  $^{129}\text{Cs}$  ( $N = 74$ ) [110] and  $^{141}\text{Pr}$  ( $N = 82$ ) [83]. The measured value of  $g$ -factor for the  $11/2^-$  state in  $^{133}\text{La}$  comes closer to that in  $^{129}\text{Cs}$ . As  $\Delta I = 2$  bands have been observed on the  $h_{11/2}$  quasiproton states in  $^{129}\text{Cs}$  and  $^{133}\text{La}$  isotopes, the  $g$ -factor of  $11/2^-$  state in  $^{133}\text{La}$  is expected to be similar to that of  $^{129}\text{Cs}$ , due to their modestly deformed even–even cores, rather than that of  $^{141}\text{Pr}$  which has a spherical core.

## 5 Future scope for the study of isomers in $A \approx 130$ and other mass regions

### 5.1 Proposed lifetime measurements in $^{135, 139}\text{La}$

For a comprehensive comparison of the half-lives across all the odd- $A$  isotopes of La in mass 130–140 region, the measurements of lifetime of the  $11/2^-$  isomeric state in  $^{135}\text{La}$  is essential. At present, a tentative upper limit of 10 ns lifetime is proposed for this level. Similarly, in  $^{139}\text{La}$ , any isomeric state with  $I^\pi = 11/2^-$  or  $23/2^+$  is not reported yet. Hence, measurement of lifetimes across such levels can be proposed.

### 5.2 Study of shape isomers in doubly-odd La isotopes

A new isomer with  $I^\pi = 14^+$  with a half-life of 187(27) ns was found at an excitation energy of around 2.3 MeV in  $^{136}\text{La}$  [15]. This is the only long-lived isomer that has been observed at high spin in odd–odd nuclei in the  $A = 130$ –140 mass region. High-spin shape isomers have already been reported in  $A \approx 150$  [115–117]. Owing to the effect of similar Fermi space in different mass regions on the evolution of isomeric states (see the subsection on isomers in different mass regions), more efforts are desired to nurture the possibilities of the existence of shape isomers in  $A \approx 130$ –140 La. Nishibata et al. opined for the structure to be similar in levels higher than  $14^+$  as no other isomer at high-spin region was found. The authors suggested a new type of collective-like structure in the  $N = 79$  region and hence, more experimental works on the high-spin states of odd–odd  $^{138}\text{La}$  and  $^{134}\text{Cs}$  was proposed to clarify the mechanism of the structural change in  $A = 130$ –140 mass region. On the other hand, Teruya et al. [118] explained that the  $14^+$  state becomes an isomer due to a band crossing of two bands with completely different configurations. In this context, nuclear moment measurement of the  $14^+$  state will be very crucial to affirm whether it is a shape isomer or spin isomer.

Further, an experimental program has been started with the BARC-TIFR PLF at TIFR, Mumbai for the study of nuclear isomers in the  $A \approx 90$  and 200 regions [119]. Since there is a similarity in occupancy of Fermi surface in these regions with respect to  $A \approx 135$ , the new effort will be helpful to develop a systematic understanding of the structure of these isomers as we move away from the shell closure.

## 6 Conclusions

The shape evolution of nuclei around  $A \approx 135$  region when one goes from  $N = 72$  to 82 remains a subject of immense interest as their systematic spectroscopic studies and isomers can provide testing of different nuclear structure models. In this context, results from the measurements of lifetime and electromagnetic moments carried out for odd- $A$  La isotopes using the hybrid array of clover HPGe and LaBr<sub>3</sub>(Ce) detectors as well as the TDPAD setup at BARC-TIFR, PLF at TIFR, Mumbai have been discussed. An overview of the comparison of the experimental results on the observed isomeric states in odd-La with large scale shell model calculations was provided. Another interesting result is the observation of enhanced  $B(E3)$  strength in  $^{137}\text{La}$  which was explained by RPA calculations. These experimental results on odd-La isotopes, along with the known isomers in the even–even Ba and Ce isotopes as well as odd-Ba and Ce isotopes, provide a broad picture of nuclear structure evolution in this region. These results show a rich variety of nuclear structure phenomena in the  $A \approx 135$  region as one goes from mid-shell to magic gap. To get a comprehensive understanding of variety of structure phenomena in La isotopes, additional measurements of the isomers in  $^{135, 136, 138, 139}\text{La}$  are being planned. We have also mentioned the ongoing measurements and future possibilities in  $A \approx 90$  and 200 region to study similar investigation of nuclear structure evolution using the setups available at our accelerator in TIFR, Mumbai.

**Acknowledgements** The authors thank Prof. E. Ideguchi, Prof. N Simuzu, Prof. Y. Utsuno, and Prof. T. Inakura for the calculations and discussion on the La isotopes. The help from Dr. Biswajit Das for the GEANT4 simulation figure of the hybrid array of Clover HPGe and LaBr<sub>3</sub>(Ce) detectors array is acknowledged. The authors would like to acknowledge the TIFR-BARC Pelletron Linac Facility for providing good quality beams. The help and cooperation from S. M. Davane, B. Naidu, S. Jadhav and R. Donthi for setting up the experimental apparatus is also acknowledged. This work is supported by the Department of Atomic Energy, Government of India (Project Identification No. RTI 4002), and the Department of Science and Technology, Government of India (Grant No. IR/S2/PF-03/2003-II). This work is partially supported by the International Joint Research Promotion Program of Osaka University. D. C. acknowledges the financial support from the Science and Engineering Research Board, Department of Science and Technology, Government of India, under Core Research Grant (Grant No. CRG/2022/005439), for this work. N. G. would like to acknowledge IIT(BHU) for the financial support. S. N. acknowledges the financial support from the SERB-DST, India under CRG (File No.: CRG/2021/006671).

**Funding** Open access funding provided by Department of Atomic Energy.

**Data availability** No data associated in the manuscript.

**Open Access** This article is licensed under a Creative Commons Attribution 4.0 International License, which permits use, sharing, adaptation, distribution and reproduction in any medium or format, as long as you give appropriate credit to the original author(s) and the source, provide a link to the Creative Commons licence, and indicate if changes were made. The images or other third party material in this article are included in the article's Creative Commons licence, unless indicated otherwise in a credit line to the material. If material is not included in the article's Creative Commons licence and your intended use is not permitted by statutory regulation or exceeds the permitted use, you will need to obtain permission directly from the copyright holder. To view a copy of this licence, visit <http://creativecommons.org/licenses/by/4.0/>.

## References

1. P.M. Walker, G. Dracoulis, *Nature* **399**, 6731 (1999)
2. S. Garg et al., *At. Data Nucl. Data Tables* **150**, 101546 (2023)
3. A.K. Jain, B. Maheshwari, A. Goel, *Nuclear Isomers: A Primer* (Springer Nature, Berlin, 2021)
4. G.D. Dracoulis, P.M. Walker, F.G. Kondev, *Rep. Prog. Phys.* **79**, 076301 (2016)
5. P.D. Bond, J.D. McGervey, S. Jha, *Nucl. Phys. A* **163**, 571–576 (1971)
6. N. Shimizu, T. Mizusaki, Y. Utsuno, Y. Tsunoda, *Comput. Phys. Commun.* **244**, 372 (2019)
7. J.T. Matta et al., *Phys. Rev. Lett.* **114**, 082501 (2015)
8. S. Biswas et al., *Phys. Rev. C* **95**, 064320 (2017)
9. S. Biswas et al., *Eur. Phys. J. A* **55**, 159 (2019)
10. A. Vogt et al., *Phys. Rev. C* **95**, 024316 (2017)
11. A. Astier et al., *Phys. Rev. C* **89**, 034310 (2014)
12. T. Alharbi et al., *Phys. Rev. C* **87**, 014323 (2013)
13. A. Astier et al., *Phys. Rev. C* **85**, 064316 (2012)
14. E. Teruya et al., *Phys. Rev. C* **92**, 034320 (2015)
15. H. Nishibata et al., *Phys. Rev. C* **91**, 054305 (2015)
16. R. Leguillon et al., *Phys. Rev. C* **88**, 044309 (2013)
17. H. Watanabe et al., *Phys. Rev. C* **79**, 064311 (2009)
18. Q.B. Chen et al., *Phys. Lett. B* **807**, 135596 (2020)
19. Md.S.R. Laskar et al., *Proc. DAE Symp. Nucl. Phys.* **63**, 1220 (2018)
20. R. Palit et al., *Nucl. Instrum. Methods Phys. Res. A* **680**, 90 (2012)
21. B. Das et al., *Proc. DAE Symp. Nucl. Phys.* **66**, 1082 (2022)
22. Md.S.R. Laskar et al., *Phys. Rev. C* **104**, L011301 (2021)
23. J.R.V. Hise et al., *Phys. Rev.* **161**, 1254 (1967)
24. E.A. Henry, N. Smith, P.G. Johnson, R.A. Meyer, *Phys. Rev. C* **12**, 1314 (1975)
25. S. Chanda et al., *Nucl. Phys. A* **775**, 153 (2006)
26. M.L. Li et al., *Eur. Phys. J. A* **28**, 1 (2006)
27. H.-E. Mahnke, *Hyperfine Interact.* **49**, 77 (1989)
28. G. Schatz, A. Weidinger, *Nuclear Condensed Matter Physics* (Wiley, New York, 1996)
29. S.N. Mishra, *J. Phys. Condens. Matter* **21**, 115601 (2009)
30. Evaluated Nuclear Structure Data File (<http://www.nndc.bnl.gov/ensdf/>); XUNDL database (<http://www.nndc.bnl.gov/ensdf/ensdf/xundl.jsp>)
31. R. Garg et al., *Phys. Rev. C* **87**, 034317 (2013)
32. J. Chen, *Nucl. Data Sheets* **146**, 1 (2017)
33. Md.S.R. Laskar et al., *Phys. Rev. C* **101**, 034315 (2020)
34. W. Witthuhn, W. Engel, *Hyperfine interactions of radioactive nuclei*, in *Topics in Current Physics*, ed. by J. Christiansen (Springer, Berlin, Heidelberg, 1983), p.205

35. M. Budzynsky et al., *Yad. Fiz.* **21**, 913 (1975); *Sov. J. Nucl. Phys.* **21**, 469 (1976)
36. W. Kohn, L.J. Sham, *Phys. Rev.* **140**, A1133 (1965)
37. E. Sjöstedt et al., *Solid State Commun.* **114**, 15 (2000)
38. P. Blaha, K. Schwarz, G.K.H. Madsen, D. Kvasnicka, J. Luitz, *WIEN2k: An Augmented Plane Wave + Local Orbitals Program for Calculating Crystal Properties* (Karlheinz Schwarz, Technische Universität (Austria, Wien, 2001)
39. K.E.G. Löbner et al., *Nucl. Data Tables* **A7**, 495–564 (1970)
40. S.N. Ghoshal, *Nucl. Phys.* (S Chand And Company Limited, New Delhi, 2018)
41. Md.S.R. Laskar et al., *Phys. Rev. C* **99**, 014308 (2019)
42. Md.S.R. Laskar et al., *Hyperfine Interact.* **240**, 96 (2019)
43. A.M. Bruce et al., *Phys. Rev. C* **55**, 620 (1997)
44. P.M. Walker et al., *Phys. Rev. Lett.* **65**, 416 (1990)
45. P.M. Walker et al., *Phys. Rev. Lett.* **67**, 433 (1991)
46. S. Frauendorf, *Nucl. Phys. A* **557**, 259c (1993)
47. P.M. Walker et al., *Nucl. Phys. A* **568**, 397 (1994)
48. N.L. Gjørup et al., *Nucl. Phys. A* **582**, 369 (1995)
49. P. Chowdhury et al., *Nucl. Phys. A* **485**, 136 (1988)
50. T. Bengtsson et al., *Phys. Rev. Lett.* **62**, 2448 (1989)
51. B. Crowell et al., *Phys. Rev. Lett.* **72**, 1164 (1994)
52. H. Rotter et al., *Nucl. Phys. A* **133**, 648 (1969)
53. F.R. Xu, P.M. Walker, R. Wyss, *Phys. Rev. C* **59**, 731 (1999)
54. T. Morek et al., *Phys. Rev. C* **63**, 034302 (2001)
55. E.S. Paul et al., *Nucl. Phys.* **619**, 177 (1997)
56. M.G. Procter et al., *Phys. Rev. C* **83**, 034311 (2011)
57. D. Ward, R.M. Diamond, F.S. Stephens, *Nucl. Phys. A* **117**, 309 (1968)
58. R.B. Firestone, *Table of Isotopes*, 8th edn. (Wiley Interscience, New York, 1996)
59. A.M. Bruce et al., *Phys. Rev. C* **50**, 480 (1994)
60. D.M. Todd et al., *J. Phys. G* **10**, 1407 (1984)
61. J. Hattula, H. Helppi, A. Luukko, *Phys. Scr.* **26**, 205 (1982)
62. K. Schiffer et al., *Nucl. Phys. A* **458**, 337 (1986)
63. L.I.U. Hong-Liang, X.U. Fu-Rong, *Chin. Phys. C* **30**, 2 (2006)
64. L.I.U. Hong-Liang, X.U. Fu-Rong, *Chin. Phys. Lett.* **25**, 1621 (2008)
65. J. Perkowski et al., *Acta Phys. Pol. B* **43**, 2 (2012)
66. J. Kaur et al., *EPJ Web of Conferences INPC 2013—International Nuclear Physics Conference*, vol. 66, p. 02058 (2014)
67. E. Dafni et al., *Hyp. Int.* **15–16**, 101 (1983)
68. T. Morek et al., *Zeitschr. Phys. A* **298**, 267–271 (1980)
69. T. Shizuma et al., *Eur. Phys. J. A* **20**, 207–210 (2004)
70. O. Hüsser et al., *Nucl. Phys. A* **279**, 287 (1982)
71. A. Berger, H.E. Mahnke, H. Grawe, W. Semmler, R. Sielemann, *Z. Phys. A* **321**, 403 (1985)
72. E. Dafni et al., *Phys. Lett. B* **181**, 1–2 (1986)
73. D. Húsar et al., *Nucl. Phys. A* **292**, 267 (1977). (**and references therein**)
74. M. B. Goldberg et al., *Proc. Intern. Conf. on Nuclear Behaviour at High Angular Momentum*, Strasbourg, p. 49 (1980)
75. A. Zemel et al., *Nucl. Phys. A* **383**, 165 (1982)
76. J.A. Sheikh et al., *Nucl. Phys. A* **824**, 58 (2009)
77. M. Müller-Veggian et al., *Proc. Int. Symp. on High-spin States and Nuclear Structure*, ed. by L. Funke (Zentralinstitut für Kernforschung, Rossendorf, Dresden, 1977), p. 19
78. C. Bell, P. Raghavan, Y. Niv, D.E. Murnick, P. Pappas, *Bull. Am. Phys. Soc.* **27**, DF10 (1982)
79. L. Kaya et al., *Phys. Rev. C* **100**, 024323 (2019)
80. M.A.J. Mariscotti et al., *Nucl. Phys. A* **311**, 395–412 (1978)
81. J.C. Merdinger et al., *Nucl. Phys. A* **346**, 281–284 (1980)
82. L. Käubler et al., *Z. Phys. A Atom. Nucl.* **329**, 143–150 (1988)
83. H. Ejiri, T. Shibata, M. Takeda, *Nucl. Phys. A* **221**, 211 (1974)
84. A.Y. Dauenhauer, K.S. Krane, *Phys. Rev. C* **85**, 064301 (2012)
85. J. Kaur et al., *Phys. Rev. C* **87**, 643011 (2013)
86. X.L. Che et al., *Eur. Phys. J. A* **30**, 347–350 (2006)
87. K. Moran et al., *Phys. Rev. C* **90**, 041303(R) (2014)
88. R.D. Hill, G. Scharff-Goldhaber, M. McKeown, *Phys. Rev.* **84**, 382 (1982)
89. J.E. Thun, S. Tomkvist, F. Falk, H. Snellman, *Nucl. Phys.* **67**, 625 (1967)
90. J. Gizon, A. Gizon, D.J. Horen, *Nucl. Phys. A* **252**, 509 (1975)
91. P. Granholms et al., *J. Phys. G Nucl. Part. Phys.* **38**, 015101 (2011)
92. P. Ring, P. Schuck, *The Nuclear Many-Body Problem* (Springer, New York, 1980)
93. S.J. Zhu et al., *Phys. Rev. C* **62**, 044310 (2000)
94. J. Gizon et al., *J. Phys. G Nucl. Phys.* **4**, L171 (1978)

95. M. Lach et al., *Z. Phys. A* **345**, 427 (1993)
96. J. Suhonen, *From Nucleons to Nucleus: Concepts of Microscopic Nuclear Theory* (Springer, Berlin, 2007)
97. S. Juutinen et al., *Phys. Rev. C* **51**, 1699 (1995)
98. L. Kaya et al., *Phys. Rev. C* **98**, 054312 (2018)
99. J. Gizon, A. Gizon, R.M. Maier, R.M. Diamond, F.S. Stephens, *Nucl. Phys. A* **222**, 557 (1974)
100. J. Gizon, A. Gizon, R.M. Diamond, F.S. Stephens, *Nucl. Phys. A* **290**, 272 (1977)
101. J. Meyer-ter-Vehn, *Nucl. Phys. A* **249**, 111 (1975)
102. M. Ionescu-Bujor et al., *Nucl. Phys. A* **633**, 459–478 (1998)
103. A. Vancraeynest et al., *Phys. Rev. C* **87**, 064303 (2013)
104. J.J. Valiente-Dobon et al., *Phys. Rev. C* **69**, 024316 (2004)
105. M. Müller-Veggian et al., *Z. Phys. A* **290**, 43 (1979)
106. B.A. Brown, W.D.M. Rae, *Nucl. Data Sheets* **120**, 115 (2014)
107. Y. Nagai, K. Hisatake, *J. Phys. Soc. Jpn.* **36**, 1501 (1974)
108. J. Genevey et al., *Phys. Rev. C* **67**, 054312 (2003)
109. H. Watanabe et al., *Mod. Phys. Lett. A* **25**, 1800 (2010)
110. M.S. Dewey et al., *Phys. Rev. C* **18**, 2061 (1978)
111. N. Shimizu et al., *Phys. Scr.* **92**, 063001 (2017)
112. T. Togashi et al., *Phys. Rev. C* **91**, 024320 (2015)
113. Y. Utsuno et al., *Phys. Rev. Lett.* **114**, 032501 (2015)
114. K. Wisshak, H. Kleve-Nebenius, D. Habs, H. Faust, *Nucl. Phys. A* **247**, 59–73 (1975)
115. Y. Gono et al., *Eur. Phys. J. A* **13**, 5–8 (2002)
116. A. Odahara et al., *Z. Phys. A* **350**, 185–6 (1994)
117. X.H. Zhou et al., *Phys. Rev. C* **61**, 014303 (1999)
118. E. Teruya et al., *Phys. Rev. C* **94**, 014317 (2016)
119. S. Singh et al., *Acta Phys. Pol. B* **17**, 3–A10 (2024)